USGS
science for a changing world

Prepared in cooperation with the U.S. Fish and Wildlife Service and the Bureau of Reclamation

Construction, Calibration, and Validation of the RBM10 Water Temperature Model for the Trinity River, Northern California

Open-File Report 2016–1056

U.S. Department of the Interior
U.S. Geological Survey

Cover: Photograph showing sunrise on the Trinity River, northern California.
Photograph by Edward C. Jones, U.S. Geological Survey, October 29, 2008.

Construction, Calibration, and Validation of the RBM10 Water Temperature Model for the Trinity River, Northern California

By Edward C. Jones, Russell W. Perry, John C. Risley, Nicholas A. Som, and Nicholas J. Hetrick

Prepared in cooperation with the U.S. Fish and Wildlife Service and the Bureau of Reclamation

Open-File Report 2016–1056

U.S. Department of the Interior
U.S. Geological Survey

U.S. Department of the Interior
SALLY JEWELL, Secretary

U.S. Geological Survey
Suzette M. Kimball, Director

U.S. Geological Survey, Reston, Virginia: 2016

Suggested citation:
Jones, E.C., Perry, R.W., Risley, J.C., Som, N.A., and Hetrick, N.J., 2016, Construction, calibration, and validation of the RBM10 water temperature model for the Trinity River, northern California: U.S. Geological Survey Open-File Report 2016–1056, 46 p., http://dx.doi.org/10.3133/ofr20161056.

ISSN 2331-1258 (online)

Contents

Figures

Tables

Conversion Factors

Inch/Pound to International System of Units

Multiply	By	To obtain
	Length	
mile (mi)	1.609	kilometer (km)
	Area	
square foot (ft^2)	0.09290	square meter (m^2)
square mile (mi^2)	2.590	square kilometer (km^2)
	Flow rate	
cubic foot per second (ft^3/s)	0.02832	cubic meter per second (m^3/s)
	Density	
kilogram per cubic meter (kg/m^3)	0.06242	pound per cubic foot (lb/ft^3)
	Energy	
Watt per meter squared (W/m^2)	0.0002389	kilocalories per meter squared per second ($kcal/m^2/s$)

International System of Units to Inch/Pound

Multiply	By	To obtain
	Length	
meter (m)	3.281	foot (ft)
meter (m)	1.094	yard (yd)
	Area	
square meter (m^2)	0.0002471	acre
square meter (m^2)	10.76	square foot (ft^2)
	Wind speed	
	Pressure	
kilopascal (kPa)	10	millibar (mb)
pascal (Pa)	0.01	millibar (mb)
millibar (mb)	0.1	kilopascal (kPa)
	Wind speed	
meter per second (m/s)		foot per second (ft/s
	Energy	
kilocalories per meter squared per second ($kcal/m^2/s$)	8,569	Langley per day (Ly/day)

Temperature in degrees Celsius (°C) may be converted to degrees Fahrenheit (°F) as °F = (1.8 × °C) + 32.

Datum

Horizontal coordinate information is referenced to the North American Datum of 1983 (NAD 83).

Abbreviations

MAE	mean absolute error
ME	mean error
NSS	Nash-Sutcliffe statistic
RBM10	River Basin Model-10
Reclamation	Bureau of Reclamation
RM	river mile
RMSE	root mean square error
USFWS	U.S. Fish and Wildlife Service
USGS	U.S. Geological Survey

Construction, Calibration, and Validation of the RBM10 Water Temperature Model for the Trinity River, Northern California

By Edward C. Jones[1], Russell W. Perry[1], John C. Risley[1], Nicholas A. Som[2], and Nicholas J. Hetrick[2]

Abstract

We constructed a one-dimensional daily averaged water-temperature model to simulate Trinity River temperatures for 1980–2013. The purpose of this model is to assess effects of water-management actions on water temperature and to provide water temperature inputs for a salmon population dynamics model. Simulated meteorological data, observed streamflow data, and observed water temperatures were used as model inputs to simulate a continuous 34-year time series of historical daily mean water temperature at eight locations along 112.2 river miles from Lewiston Dam near Weaverville, California, downstream to the Klamath River confluence. To demonstrate the utility of the model to inform management actions, we simulated three management alternatives to assess the effects of bypass flow augmentation in a drought year, 1994, and compared those results to the simulated historical baseline, referred to as the "No Action" alternative scenario. Augmentation flows from the Lewiston Dam bypass consist of temperature-controlled releases capable of cooling downstream water temperatures in hot times of the year, which can reduce the probability of disease outbreaks in fish populations. Outputs from the Trinity River water-temperature model were then used as inputs to an existing water-temperature model of the Klamath River to evaluate the effect of augmentation flow releases on water temperatures in the lower Klamath River.

We structured the Trinity River water-temperature model in River Basin Model-10 (RBM10), which uses a simple equilibrium flow model, assuming discharge in each river segment on each day is transmitted downstream instantaneously. The model uses a heat-budget formulation to quantify heat flux at the air-water interface. Inputs for the heat budget are calculated from daily mean meteorological data, including net shortwave solar radiation, net longwave atmospheric radiation, air temperature, wind speed, vapor pressure, and a psychrometric constant needed to calculate the Bowen ratio. The modeling domain was divided into eight reaches ranging in length from 8.8 to 20.6 miles, which were calibrated and validated separately with observed water temperature data collected irregularly from 1980 to 2013. Root mean square errors of observed and simulated water temperatures for the eight reaches ranged from 0.25 to 1.12 degrees Celsius (°C). Mean absolute errors ranged from 0.18 to 0.89 °C. For model validation, a *k*-fold cross-validation technique was used. Validation root mean square error and mean absolute error for the eight reaches ranged from 0.24 to 1.11 °C and from 0.18 to 0.89 °C, respectively.

[1]U.S. Geological Survey.

[2]U.S. Fish and Wildlife Service.

Augmentation scenarios were based on historical hydrological and meteorological data, combined with prescribed flow and temperature releases from Lewiston Dam provided by the Bureau of Reclamation. Water releases were scheduled to achieve targeted flows of 2,500, 2,800, and 3,200 cubic feet per second in the lower Klamath River from mid-August through late September, coinciding with the upstream migration of adult fall-run Chinook salmon (*Oncorhynchus tshawytscha*). Water temperatures simulated at river mile 5.7 on the Klamath River showed a 5 °C decrease from the No Action historical baseline, which was near or greater than 23 °C when augmentation began in mid-August. Thereafter, an approximate 1 °C difference among augmentation scenarios emerged, with the decrease in water temperature commensurate to the level of augmentation. All augmentation scenarios simulated water temperatures equal to or less than 21 °C from mid-August through late September. Water temperatures equal to or greater than 23 °C are of particular interest because of a thermal threshold known to inhibit upstream migration of salmon. When temperatures exceed this approximate 23 °C threshold, Chinook salmon are known to congregate in high densities in thermal refugias and show extended residence times, which can potentially trigger epizootic outbreaks such as of *Ichthyophthirius multifiliis* ("Ich") and *Flavobacterium columnare* ("Columnaris") that were the causative factors of the Klamath River fish kill in 2002. A model with the ability to simulate water temperatures in response to management actions at the basin scale is a valuable asset for water managers who must make decisions about how best to use limited water resources, which directly affect the state of fisheries in the Klamath Basin.

Introduction

Water temperature influences important life-cycle parameters of fish populations such as survival and growth rates, which in turn dictate population dynamics. Fisheries and water managers are interested in understanding the effects of management actions on water temperature, and consequent effects on Pacific salmon (*Oncorhynchus* spp.) downstream of dams in the Klamath Basin. Aquatic research tools used to understand these relationships often include water-temperature modeling, fish life-cycle modeling, and mark-capture analyses (Perry and others, 2010, 2012, 2013; Plumb and others, 2012; Benjamin and others, 2013). A water temperature model typically is developed first because it is used as input to fish life-cycle models.

We present a water temperature model for the Trinity River, a major tributary to the Klamath River. Our model uses publically available simulated meteorological data and observed streamflow data to estimate daily mean water temperature. Previous water-temperature modeling studies of the Trinity River include Zedonis (1997), Deas (1998, 2002), and Watercourse Engineering (2007). We structured our model in River Basin Model-10 (RBM10; Yearsley, 2003, 2009) to be compatible with the RBM10 model for the Klamath River developed by Perry and others (2011). Once calibrated and validated, the Trinity River model will be linked to the Klamath River RBM10 model to form a single model, thereby providing a unified framework for water temperature and salmon life-cycle models in the Klamath Basin. Simulated temperatures from the integrated Klamath/Trinity water temperature model will provide critical inputs to the Stream Salmonid Simulator (S^3; Russell Perry, U.S. Geological Survey, unpub.), a model being developed to simulate juvenile salmon production in the Trinity River.

Our goal was to develop a model that accurately simulates daily mean water temperature along the course of the Trinity River, from Lewiston Dam (RM 112.2) to the Klamath River confluence. Simulated water temperatures from this model will be incorporated in a population model of Trinity River salmon as a basis to evaluate alternate management actions affecting salmon populations. Salmon population dynamics are affected by water temperature in many crucial ways—for example, egg

incubation rates, individual growth rates, migration timing, and disease susceptibility. The development of the RBM10 for the Trinity River is described in detail in this report. Observed water temperatures at eight locations along the river were used to calibrate the model, and the calibration and model validation results are presented. The calibrated model is then used to assess the effects of flow augmentation scenarios on water temperature in the lower Klamath River.

Study Site

The Trinity River, a major tributary of the Klamath River in northern California, has a drainage basin area of 2,970 mi^2 (fig. 1). Elevation in the drainage basin ranges from 190 ft at the confluence to 9,020 ft at its highest point, and includes parts of the Coast Ranges and Klamath Mountains. In the early 1960s, the Bureau of Reclamation (Reclamation) completed Trinity Dam (RM 120) and Lewiston Dam (RM 112.2) near Weaverville, California, as part of a system of dams and canals to provide a stable supply of irrigation water to California's Central Valley. The auxiliary outflow works at Trinity Dam provides an optional temperature-controlled release point for outflow, which bypasses the powerhouse. Bypass allows access to the colder hypolimnion, which is then discharged from Trinity Dam into Lewiston Reservoir, making cold water augmentation to the Trinity River possible at Lewiston Dam. The river from Lewiston Dam downstream to the Klamath River confluence, with parts of tributaries included, was designated as the Trinity Wild and Scenic River by the U.S. Congress in 1981.

Methods

Structure of River Basin Model 10

RBM10 is a one-dimensional water-temperature model that simulates daily mean water temperatures along the longitudinal profile of a river, based on a heat-budget formulation (Yearsley and others, 2001; Yearsley, 2009; Perry and others, 2011). The model structure and inputs are comprised of: (1) river geometry, (2) boundary conditions, and (3) meteorological data. The geometry of the Trinity River is defined by a series of river segments, each with a distinct set of continuity equations that characterize system hydraulics and geomorphic properties such as wetted channel width, depth, and water velocity as a function of stream discharge. Boundary conditions of the model are defined by major heat advection sources to the mainstem Trinity River, represented as daily inputs of discharge and water temperature from headwaters and tributaries. Based on river geometry and boundary conditions, RBM10 applies an equilibrium flow model that assumes streamflow passes instantaneously downstream, segment-to-segment, on a daily time-step. Heat-budget computations require daily inputs of meteorological data. Given these key model components, water temperatures are simulated using a mixed Eulerian-Lagrangian numerical scheme that is computationally efficient and accurate (Yearsley, 2009). In the Lagrangian frame of reference, the heat-budget model takes the following form:

$$\frac{dT}{dt} = \frac{1}{\rho C_{\mathrm{p}} A_x}\left(W_x H_{\text{air-water}} + S_{\text{adv}}\right) \tag{1}$$

where

T is water temperature (degrees Celsius),
t is time,
ρ is the density of water (kilograms per cubic meter),
C_{p} is the specific heat capacity of water (kilocalories per degree Celsius per kilogram),

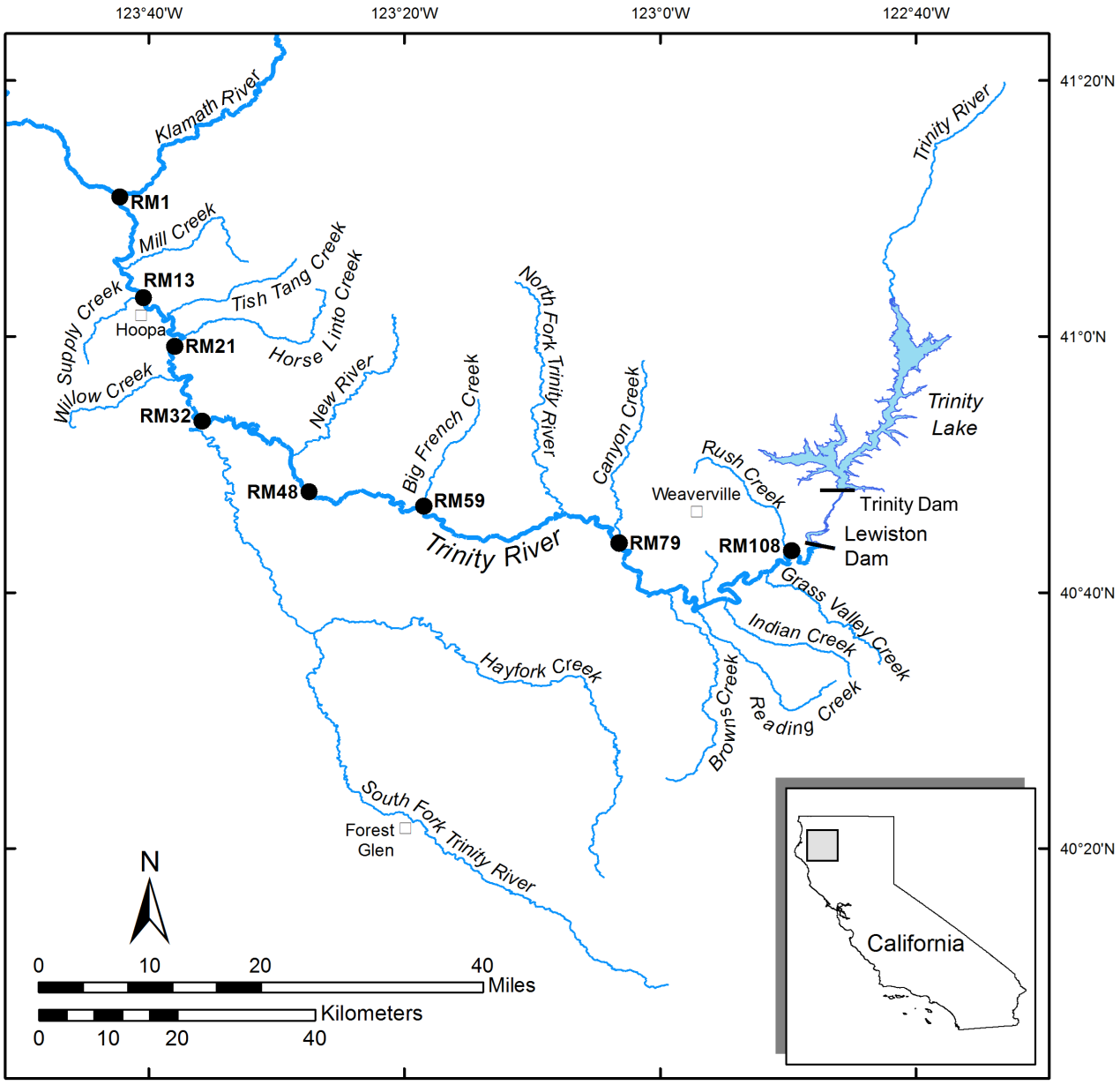

Figure 1. Map showing eight locations (circles) where observed water temperature data were measured and used to calibrate RBM10 at the downstream end of each meteorological reach of the Trinity River drainage basin, northern California.

A_x is the cross-sectional area of the river (square meters) at location x along the river's longitudinal axis,

W_x is the width of the river (meters) at location x,

$H_{\text{air-water}}$ is the net heat flux at the air-water interface (kilocalories·per meter squared per second), and

S_{adv} is heat advected from tributaries (kilocalories·per meter squared per second).

River Geometry

To model the hydraulic properties of the Trinity River, the geometry of river segments in RBM10 is characterized by wetted channel width and cross-sectional area, both of which vary with river discharge. Continuity equations were used to quantify these relationships:

$$W_x = a_{\text{W}} Q^{b_{\text{W}}}, \tag{2}$$

$$A_x = a_{\text{A}} Q^{b_{\text{A}}}, \tag{3}$$

where

W_x and A_x are wetted top width (feet) and cross-sectional area (square feet), respectively, for the segment beginning at river mile x,

Q is discharge (cubic feet per second), and

a and b are segment-specific parameters that need to be estimated.

We formed 31 river segments for RBM10, each of which had unique parameters of the continuity equations. Segment breaks were defined based on location of tributaries and changes in bed slope such that each segment had a relatively constant average slope (mean reach length = 3.6 mi, range = 1.2–5.6 mi; table A1). One segment (RMs 93.9–92.6) was later partitioned into two segments so that each segment contained no more than one input tributary.

To estimate reach-specific parameters of the continuity equations, a HEC-RAS model (U.S. Army Corps of Engineers, 2010) for the Trinity River was used to simulate wetted top-width and cross-sectional area for 112.2 river miles from Lewiston Dam (RM 112.2) to the Klamath River confluence (RM 0). For the upper 40 mi extending from the dam to the North Fork Trinity River (RM 72.2), HEC-RAS geometry data were available from a flood insurance study by the California Department of Water Resources (2014). The HEC-RAS geometry consisted of 785 cross-sectional elevation profiles over the 40 mi of river channel and was compiled from bathymetric, lidar (light detection and ranging), and ground survey data. From the North Fork Trinity River confluence to the Klamath River, we used river geometry from a water-temperature model developed by Watercourse Engineering, Inc. (2007). Geometry from this model consisted of 1,168 cross-sectional elevation profiles over the 72.2 mi of river, which was constructed from a series of four different trapezoidal shapes to represent the channel profile. Geo-referenced cross-sectional profiles from both data sources were used to develop a single HEC-RAS model. This model was then used to simulate wetted channel top-width and cross-sectional area for each cross section at 15 exceedance flows, ranging from 2 to 100 percent of the 10-year exceedance flow (range = 801– 40,040 ft^3/s at the Klamath River confluence). To estimate parameters of the continuity equations (a_W, b_W, a_A, and b_A) for each river segment in the RBM10 model, linear models of the form $\ln(y) = \ln a + b\ln Q$ were fit to top width and cross-sectional area for each river segment. These estimates defined the average hydraulic conditions for each of the original 31 river segments in the RBM10 river geometry (table A1).

Meteorological Data

Heat flux at the water surface is quantified by the simplified heat-budget formula of RBM10 (Yearsley and others, 2001; Yearsley, 2003, 2009; Perry and others, 2011):

$$H_{\text{air-water}} = H_{\text{sw}} + \left(H_{\text{a}} - H_{\text{ar}}\right) + H_{\text{evap}} + H_{\text{cond}} + H_{\text{back}} \quad (4)$$

where

$H_{\text{air-water}}$ is the net exchange of thermal energy across the air-water interface,
H_{sw} is shortwave solar radiation incident at the water surface,
H_{a} is longwave atmospheric radiation incident at the water surface,
H_{ar} is reflected longwave atmospheric radiation,
H_{evap} is evaporative heat flux,
H_{cond} is conductive heat flux, and
H_{back} is longwave back radiation from the water surface.

Standard meteorological data on a daily time scale are required to compute the heat budget. Shortwave solar radiation incident at the water surface (H_{sw}) and net longwave atmospheric radiation (H_{a} - H_{ar}) are direct inputs to RBM10, whereas the other heat-budget terms are calculated internally from inputs of daily mean air temperature (in degrees Celsius), daily mean wind speed (in meters per second), vapor pressure (in millibars), and a psychrometric constant needed to calculate the Bowen ratio (Yearsley and others, 2001; Yearsley, 2009). Cloud cover was used to estimate net longwave radiation. Meteorological inputs to RBM10 are spatially explicit, to account for the gradient in climate across the river's longitudinal profile. We delineated eight meteorological reaches, each with a unique set of meteorological input data (tables A1 and A2). Reach definitions were influenced by the availability of sites with a sufficient record of water temperature measurements for model calibration of evaporation coefficients. Meteorological reaches ranged in length from 8.8 to 20.6 mi.

In the absence of long time series of meteorological data from weather stations along the Trinity River, model inputs were constructed from simulated meteorological data. We compiled a 34-year daily historical record of meteorology from 1980 through 2013. Time series of daily minimum and maximum air temperature (in degrees Celsius), shortwave solar radiation (in Watts per meter squared), daylight (in seconds per day), and vapor pressure (in pascals) were extracted from the 1 × 1 km spatial grid of Daymet (Thornton and others, 1997, 2000, 2014; Thornton and Running, 1999) at the midpoint of each of the eight model reaches (see table A2 for latitude-longitude coordinates). Daily mean air temperature was calculated as the mean of the minimum and maximum daily air temperature. We computed cloud cover from daily mean air temperature following methods described in Flint and Flint (2008). Time series of daily mean wind speed (in meters per second) were extracted at the same eight locations (table A2), from a spatial grid of 1/16-degree resolution available from Livneh and others (2015).

Shortwave solar radiation, H_{sw}, was converted from units of watts per meter squared during daylight periods to kilocalories per meter squared·per second over the 24-hour period for input to RBM10. When compared to shortwave solar radiation observed at Hoopa, California (latitude, 41.0478; longitude, 123.6714; Western Regional Climate Center, 2015), the Daymet simulated data for that model reach (Reach 7) matched the observed signature reasonably well (fig. 2).

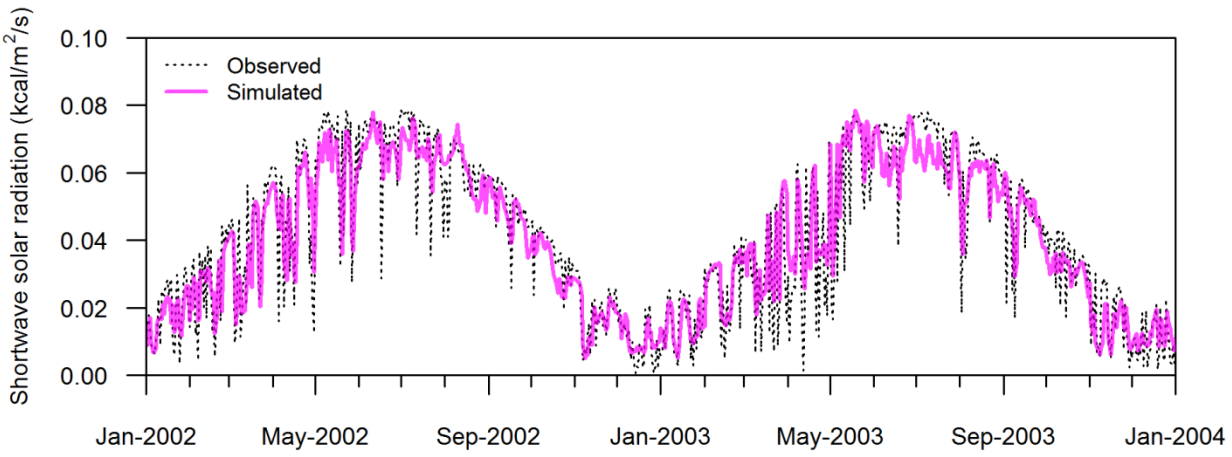

Figure 2. Graph showing observed shortwave solar radiation at Hoopa, California, and simulated shortwave solar radiation extracted from the 1 × 1 km spatial grid of Daymet, 2002–03. (kcal/m^2)/s, kilocalories per meter squared·per second.

Longwave atmospheric radiation incident at the water surface (H_a) was calculated using the Stefan-Boltzmann law:

$$H_a = \varepsilon_{eff} \sigma T_a^4, \tag{5}$$

where

ε_{eff} is the effective emissivity of the atmosphere,
σ is the Stefan-Boltzmann constant, and
T_a is daily mean air temperature (kelvins)

We used the model of Ångström (1918) for ε_{eff} as recommended by Flerchinger and others (2009), who compared estimates from different algorithms for longwave radiation to observed longwave radiation at 21 sites across North American and China:

$$\varepsilon_{clr} = 0.83 - 0.18 \times 10^{-0.067 e_a}, \tag{6}$$

where

e_a is vapor pressure (kilopascals).

Effective emissivity was then calculated by adjusting clear-sky emissivity for cloud cover using the model of Unsworth and Monteith (1975):

$$\varepsilon_{eff} = (1 - 0.84c)\varepsilon_{clr} + 0.84c, \tag{7}$$

where

c is the fraction of the sky covered by clouds.

Reflected longwave radiation was calculated as $H_{ar} = H_a A_{ar}$, where A_{ar} is longwave reflectivity, which was set to 0.03.

All other components of the heat budget were calculated as described by Yearsley and others (2001) and Yearsley (2009), although it is useful to repeat the formulation of the evaporative heat flux because this term contains parameters required to calibrate RBM10:

$$H_{\text{evap}} = \rho L_v f(W)(e_0 - e_a), \tag{8}$$

where

ρ is the density of water (kilograms per cubic meter),

L_v is the latent heat of vaporization (kilocalories per kilogram),

$f(W)$ is a function of wind speed (W), and

e_0 is the saturation vapor pressure at the temperature of the water surface (millibars).

The wind speed function often takes the general form:

$$f(W) = a + bW + cW^2 \tag{9}$$

where

a, b, and c are empirical coefficients (Edinger and others, 1974).

The specific form of $f(W)$ varies widely among studies (Edinger and others, 1974; Henderson-Sellers, 1986). For example, Yearsley and others (2001) used the simplest form for $f(W)$, assuming $a = 0$ and $c = 0$; they then estimated *b* through calibration. Coefficients of the wind speed function are calibration parameters in RBM10 (see section, "Calibration and Validation").

Boundary Conditions

Daily values of river discharge and water temperature must be provided at all boundaries where significant discharge enters the mainstem Trinity River. In addition to inputs for Lewiston Dam, we included the 14 tributaries as boundary conditions to RBM10 (table 1). Daily mean streamflow data for U.S. Geological Survey (USGS) streamgage 11525500 downstream of Lewiston Dam were used as the upstream boundary to the water-temperature model. All other boundary conditions were specified by assuming the difference in streamflow measured between streamgage 11525500 and USGS streamgage 11530000 at Hoopa, California, represented the aggregate total inflow from all tributaries. To estimate the daily mean discharge of each tributary, the daily total inflow was then partitioned among tributaries in proportion to drainage basin area.

We assembled time series of observed daily water temperature for each boundary in our model (table 1); however, a complete time series was not available (fig. 3). To fill data gaps in the 34-year time series, we used a regression model that predicts weekly mean stream temperature as a function of weekly mean air temperature (Mohseni and others, 1998):

$$T_s = \mu + \frac{\alpha - \mu}{1 + e^{\gamma(\beta - T_a)}}, \tag{10}$$

Table 1. Source of input datasets for statistical models used to estimate boundary water temperatures for the Trinity River.

[**Source:** Reclamation, Bureau of Reclamation; CDEC, California Data Exchange Center; HVT, Hoopa Valley Tribe; USFS, U.S. Forest Service; USFWS, U.S. Fish and Wildlife Service; USGS, U.S. Geological Survey. Data from Indian Creek were used as a surrogate for Reading Creek, which lacked a water temperature record. **Station ID:** A field identifier to distinguish the source data]

Tributary	Data Extent	Source	Station ID	Latitude	Longitude
Trinity River at Lewiston	1964–1983	USGS/Reclamation	11525500	40.7247	-122.8011
	1987–1990	USFWS	LWS	--	--
	1990–2015	CDEC	LWS	40.6855	-122.9342
Rush Creek	2002–2004	USFWS	RCTR1	40.7208	-122.8403
	2011–2013	USFS	rush1_H2O_Temp	40.7914	-122.8825
Grass Valley Creek	2004–2006	USGS	11525630	40.6867	-122.8600
	2004–2013	CDEC	GVT	40.6867	-122.8600
Indian Creek	2002–2013	USFWS	ICTR1	40.7267	-122.7942
Weaver Creek	2000–2006	CDEC	WVC	40.7193	-122.8036
Reading Creek				--	--
Browns Creek	2000–2012	USFS	Browns_H2O_temp	40.6260	-122.9591
Canyon Creek	2001–2013	USFWS	CNTR1	40.7308	-123.0533
	2005–2005	CDEC	CJC	40.7403	-123.0492
North Fork Trinity River	2001–2013	USFWS	NFTR1	40.7708	-123.1283
Big French Creek	2001–2013	USFWS	BFTR1	40.7803	-123.3083
New River	2005–2005	USFS	New River at Trinity River H2O temp	40.8459	-123.4799
	2011–2013	USFS	H2O_Temp_new1	40.9632	-123.3482
South Fork Trinity River	2001–2013	USFWS	SFTR1	40.8894	-123.6028
Willow Creek	1995–2003	USFS	Willow_MigrantTrap_nearmouth_H2O_temp	40.9436	-123.6324
Horse Linto Creek	1992–1993	USFS	Near confluence ("HLINTO.wk3")	--	--
	1994–1994	USFS	Near confluence ("HL94.wk3")		
	1997–2012	USFS	HorseLinto_lowerbridge_H2O_temp	41.0052	-123.6071
	2005–2006	USFS	H2O_Temp_AREMP_CALIN	41.0052	-123.6062
Tish Tang Creek	2004–2013	HVT	LTISHTANG	--	--

where

T_s is the weekly-mean stream temperature,

μ is the minimum water temperature,

α is the maximum water temperature,

β is the air temperature at the point of inflection,

γ represents the slope at the inflection point, and

T_a is the weekly mean air temperature (degrees Celsius).

The parameters μ, α, β, and γ were estimated by least-squares regression using an optimization routine in the R statistical package (R Core Team, 2014). Weekly mean air temperatures for a tributary entering a given model reach were computed from the daily mean air temperatures of that reach. Following Mohseni and others (1998), we fit separate relationships to the rising and falling limb (that is, the part of the year when air temperature tends to increase or decrease; figs. 4-6). Given parameter estimates for the rising and falling limb of each stream (table 2), we then filled data gaps by predicting daily water temperature using a 7-day moving average of air temperature. No observed water temperature data were available for Reading Creek. Due to proximity, similarities in basin size and geomorphology, we used Indian Creek as a surrogate for observed water temperatures of Reading Creek.

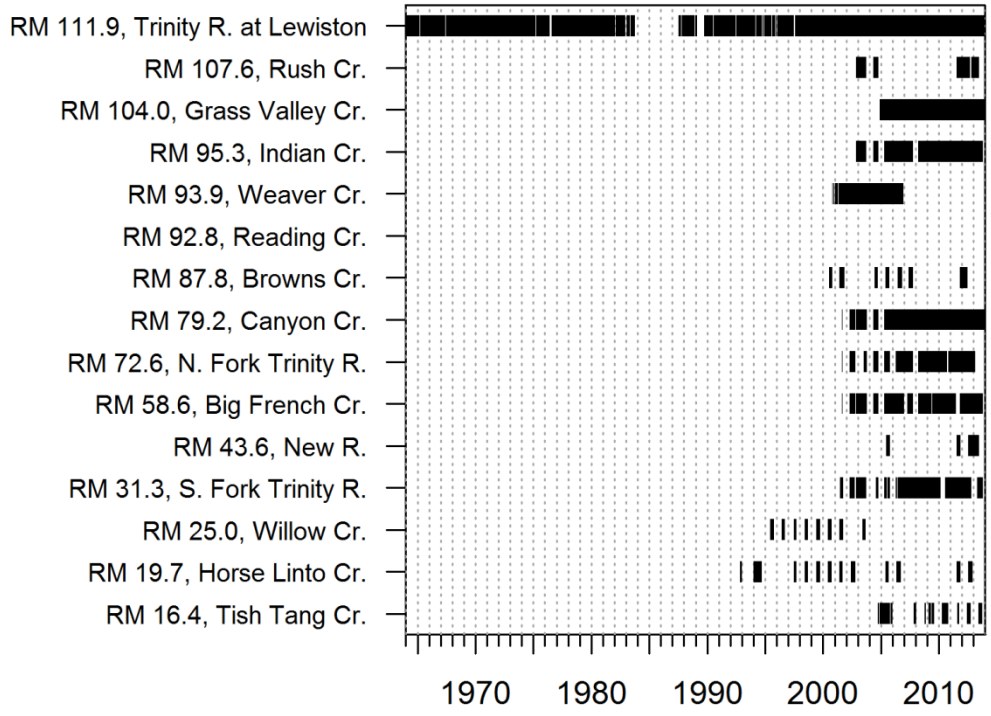

Figure 3. Graph showing extent of observed water temperature data for tributary inputs, at specified river miles (RMs), to the Trinity River. Horizontal bars represent the chronological range of available data for each tributary. Data for Indian Creek were used as a surrogate for Reading Creek, which lacked a water temperature record. Data prior to 1980 were not used because of a lack of corresponding meteorological data.

Table 2. Parameter estimates of the non-linear regression model (Mohseni and others, 1998) used to estimate water temperature for headwater and tributary inputs to the Trinity River.

Tributary	Meteorological reach	Limb	First week of limb	Minimum water temperature μ	Maximum water temperature α	Air temperature at the point of inflection β	Slope at inflection point γ
Trinity River at Lewiston	1	rising	51	8.7	19.3	-0.2	0.156
		falling	30	4.8	23.2	14.1	0.032
Rush Creek	1	rising	51	-7.1	35.1	29.0	0.092
		falling	30	4.4	23.6	11.4	0.153
Grass Valley Creek	1	rising	51	-14.0	42.0	38.9	0.056
		falling	30	-0.2	28.2	17.9	0.072
Indian Creek	1	rising	51	1.3	26.7	16.4	0.131
		falling	30	2.4	25.6	13.1	0.133
Weaver Creek	2	rising	51	-7.0	35.0	23.5	0.099
		falling	30	-3.9	31.9	19.1	0.105
Reading Creek	2	rising	51	1.4	26.6	16.0	0.136
		falling	30	2.3	25.7	13.1	0.135
Browns Creek	2	rising	51	4.6	23.4	14.0	0.207
		falling	30	3.8	24.2	14.7	0.170
Canyon Creek	3	rising	51	-22.0	50.0	35.4	0.082
		falling	30	1.6	26.4	12.0	0.167
North Fork Trinity River	3	rising	51	-14.0	42.0	28.7	0.095
		falling	30	0.3	27.7	14.2	0.154
Big French Creek	4	rising	51	-0.5	28.5	17.4	0.114
		falling	30	2.4	25.6	12.7	0.145
New River	5	rising	51	2.4	25.6	14.0	0.181
		falling	30	-7.8	35.8	21.3	0.126
South Fork Trinity River	6	rising	51	-2.2	30.2	15.0	0.178
		falling	30	-1.0	29.0	13.4	0.185
Willow Creek	6	rising	51	-3.9	31.9	20.7	0.101
		falling	30	-1.0	29.0	16.1	0.097
Horse Linto Creek	7	rising	51	-6.5	34.5	24.3	0.093
		falling	30	3.3	24.7	12.0	0.157
Tish Tang Creek	7	rising	51	1.7	26.3	15.7	0.132
		falling	30	3.1	24.9	11.9	0.161

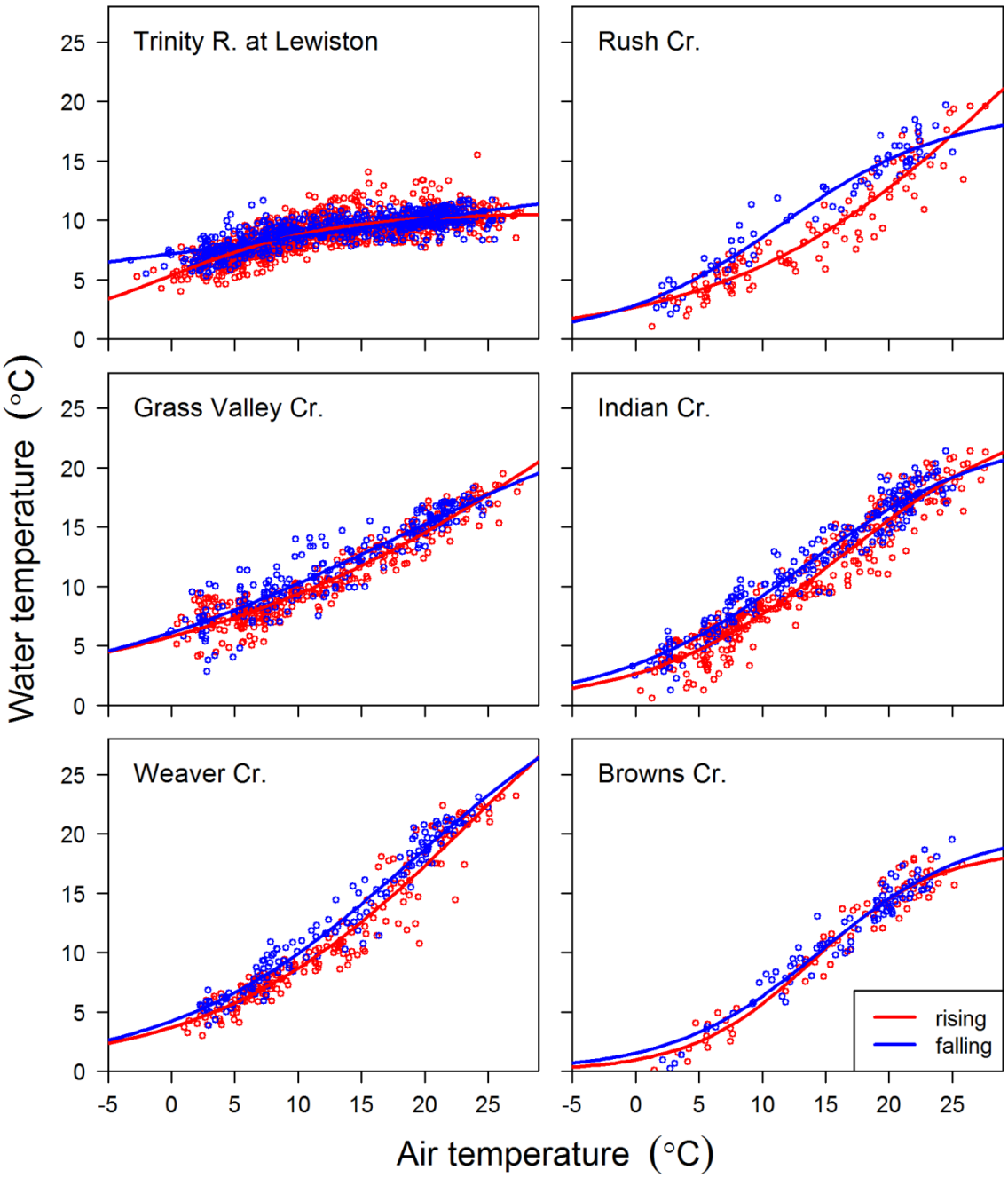

Figure 4. Scatter plots of observed weekly mean water temperature and weekly mean air temperature for six headwater and tributary inputs between river miles 111.9 and 87.8 of the Trinity River. Two lines in each panel represent the fitted non-linear regression model (Mohseni and others, 1998) used to predict water temperatures for rising and falling limbs of air temperature.

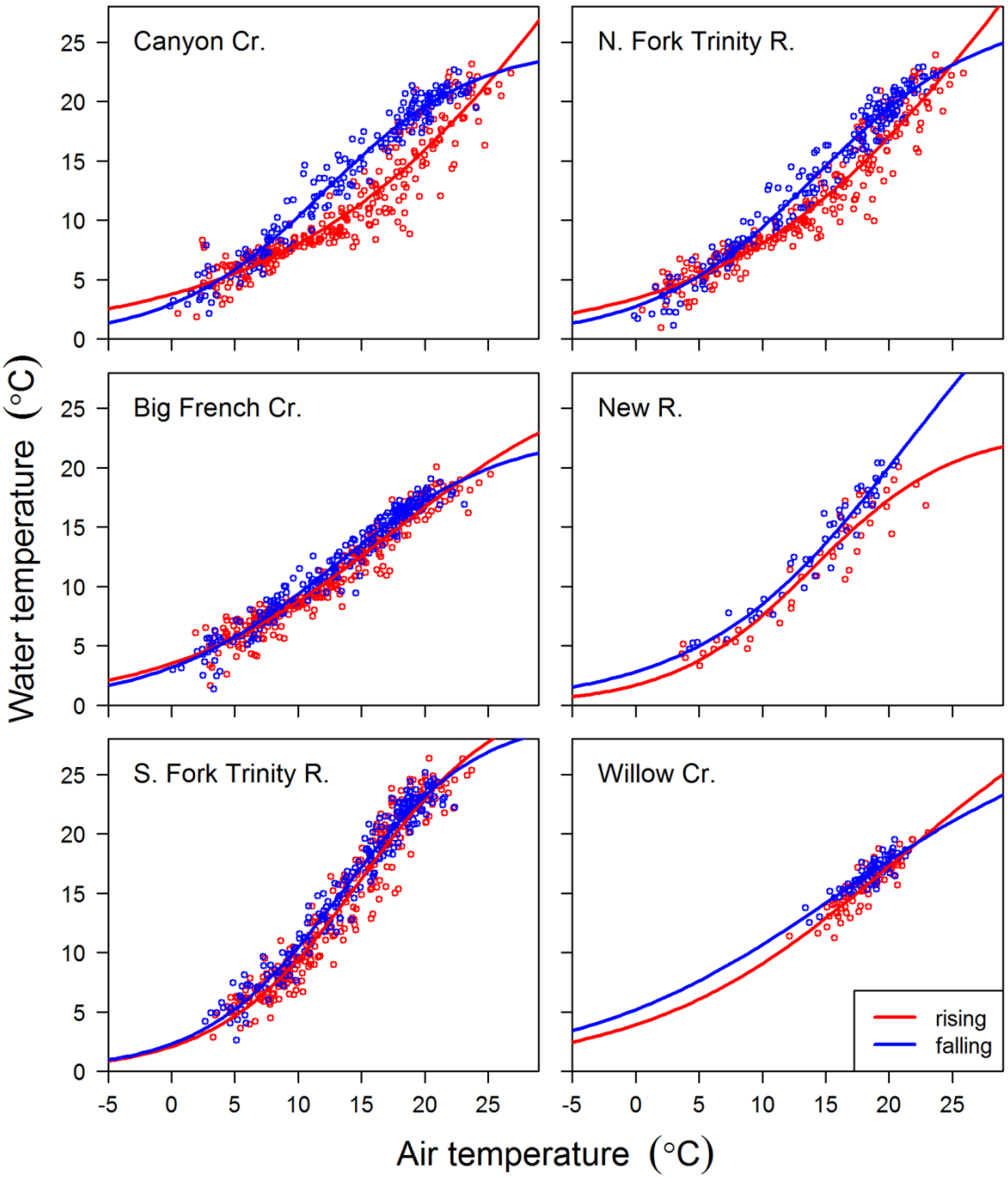

Figure 5. Scatter plots of observed weekly mean water temperature and weekly mean air temperature for six tributary inputs between river miles 79.2 and 25.0 of the Trinity River. Two lines in each panel represent the fitted non-linear regression model (Mohseni and others, 1998) used to predict water temperatures for rising and falling limbs of air temperature.

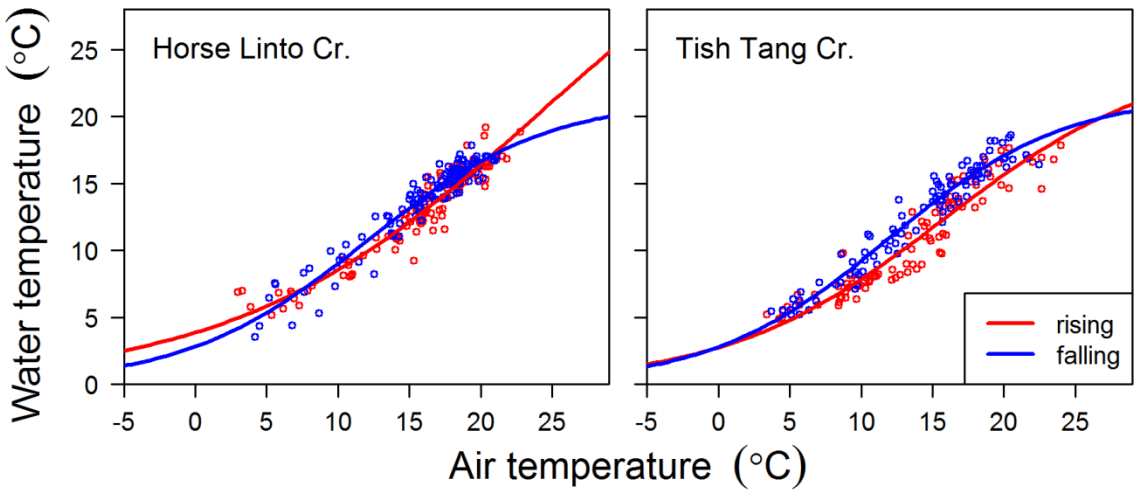

Figure 6. Scatter plots of observed weekly mean water temperature and weekly mean air temperature for two tributary inputs between river miles 19.7 and 16.4 of the Trinity River. Two lines in each panel represent the fitted non-linear regression model (Mohseni and others, 1998) used to predict water temperatures for rising and falling limbs of air temperature.

Calibration and Validation

Calibration parameters of RBM10 include coefficients that influence how wind speed affects evaporative heat flux. Heat lost through evaporation is proportional to the wind speed function, $f(W)$, and to the vapor pressure deficit, $e_0 - e_a$ (eq. 8). We assessed the fit of the water-temperature model to observed data using two forms of the wind function. First, we used a common form of the wind speed function,

$$f(W_r) = a_r + b_r W_r, \tag{11}$$

where

r is reach 1,…, 8 corresponding to each unique set of meteorological data.

Observed temperatures at eight locations along the river were close to the end points for each reach (fig. 7, tables A1 and A2), providing a direct correspondence among observed water temperature data, meteorological data, and wind-function parameters. To calibrate the model, we used an optimization routine to find parameter values of a_r and b_r that minimized the sum of squared deviations between simulated and observed temperatures. We calibrated one reach at a time, from upstream to downstream, because water temperatures at the end of reach r form the boundary conditions at the start of reach r+1. For example, observed water temperatures at the end of reach 1 were used to estimate a_1 and b_1. Next, a_1 and b_1 were set to their best-fit values and observed water temperatures at the end of reach 2 were used to estimate a_2 and b_2, and so on.

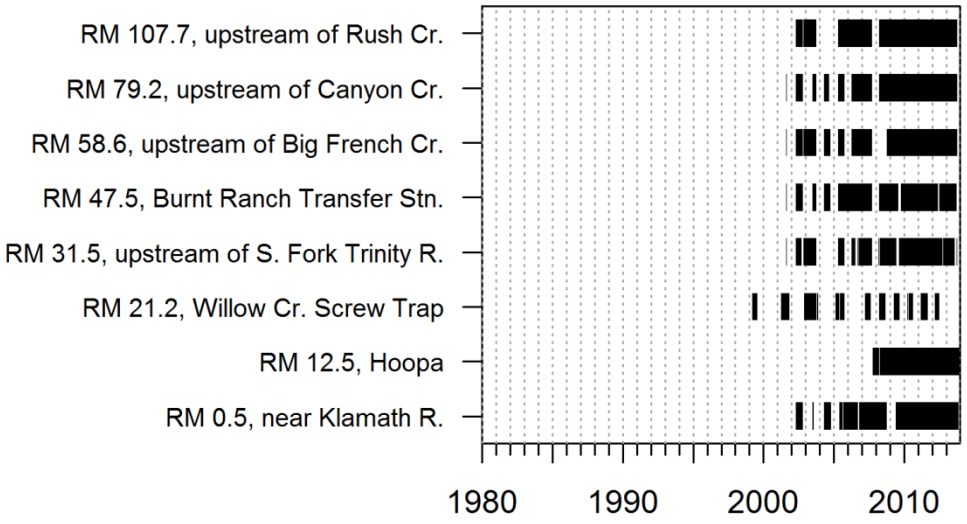

Figure 7. Graph showing extent of observed water temperature for calibrating evaporation coefficients of RBM10 at eight locations (RM, river mile) along the Trinity River. Horizontal bars represent the chronological range of available data for each tributary.

We also calibrated the water-temperature model using a wind speed function with seasonal evaporation coefficients similar to the approach of Deas and Orlob (1999):

$$f\left(W_r\right)=\begin{cases} a_{r,1}+b_{r,1}W_r & \text{if April 1} \le d \le \text{November 1} \\ a_{r,2}+b_{r,2}W_r & \text{if November 1} < d < \text{April 1} \end{cases} \tag{12}$$

where

d is the day of year and

$a_{r,j}$ and $b_{r,j}$, $\left(j=\{1,2\}\right)$ are coefficients that apply to either the period April 1 to November 1 ("summer") or November 1 to April 1 ("winter").

Based on initial calibration results, we incorporated an additional calibration parameter that scaled the heat flux at the air-water interface. Initial calibrations indicated that the best-fit parameters of the evaporation function were near zero, suggesting that the calibration was minimizing evaporative cooling in an effort to increase simulated water temperatures. Despite minimal evaporative cooling, simulated water temperatures were negatively biased. The model appeared to capture the timing of fluctuations in temperature well, suggesting that the advection of heat was being simulated accurately. Therefore, we introduced an additional calibration parameter, θ_r, that scaled the effect of water depth on heat exchange at the water surface in the water-temperature model (see eq. 1):

$$\frac{dT}{dt}=\frac{1}{\rho C_p}\left(\frac{H_{\text{air-water}}}{\theta_r D_x}+\frac{S_{\text{adv}}}{A_x}\right) \tag{13}$$

where

D_x is the average depth of the river channel at location x.

The parameter, θ_r, was also reach-specific and estimated simultaneously with the evaporation parameters for each reach.

All available data were used for calibration so that parameters were estimated across a wide range of annual variation in weather and hydrology. We assembled an extensive dataset comprised of 23,565 measurements of daily mean water temperatures with 7–13 years of data at each site (fig. 7). Observed water temperature data used in calibration were acquired from U.S. Fish and Wildlife Service (USFWS), Arcata, California, except for data from streamgage 11530000 at Hoopa, California, which was sourced from the U.S. Geological Survey National Water Information System.

We used statistical and graphical methods to determine model fit and to compare the two models with different wind functions (eqs. 11 and 12). Goodness-of-fit statistics included the root mean square error (RMSE), mean error (ME), mean absolute error (MAE), and the Nash-Sutcliffe statistic (NSS). To assess systematic departures of the model, we plotted observed and simulated water temperatures and residuals versus observed water temperatures. We compared model fit between wind functions and then selected the wind function that yielded the minimum bias and error for use in all subsequent water temperature simulations.

To evaluate model simulations with data not used to fit the model, we used *k*-fold cross validation (Davison and Hinkley, 1997). This technique involves (1) splitting the calibration dataset into $k = 1,\ldots, K$ subsets; (2) leaving out the *k*th subset (the "assessment set") while the remaining data (the "training set") are used to estimate the model parameters; and then (3) using the parameter estimates from the training set to simulate water temperatures of the assessment set. This process is repeated for all *K* subsets, goodness-of-fit statistics for each assessment set are calculated, and then an aggregate measure of fit is calculated as the mean of a particular statistic over all subsets. For our cross-validation, we split the calibration dataset into subsets by reach and year and conducted a cross-validation for each reach. The best-fit parameters estimated during the calibration process were used as initial values. Following the three steps described above, we then set aside observed data from year *k* in reach *r*, used the remaining data to estimate $a_{r,-k}$ and $b_{r,-k}$ (where -*k* indicates exclusion of the *k*th year), and then simulated water temperatures for year *k* in reach *r* using estimates of $a_{r,-k}$ and $b_{r,-k}$. Because the *K* subsets were unequal in size due to missing data in some years, we used a weighted average of the goodness-of-fit statistics with weights equal to the fraction of the observations in the *k*th year.

Simulating Management Scenarios

We used RBM10 to simulate water temperatures under three flow augmentation scenarios to demonstrate how the model can be used to assess potential water-management decisions. The goal of these scenarios was to evaluate how cold water released at Lewiston Dam would influence water temperatures in the lower Klamath River during the severe drought of 2015, under the planned operational schedule at Iron Gate Dam. Because the constructed model inputs limited our simulations to 1980–2013, we selected 1994 as a surrogate year with drought conditions similar to those of 2015 in terms of meteorology and river flows.

To simulate water temperatures in the lower Klamath River, we used the Trinity River RBM10 model and the Klamath River RBM10 model of Perry and others (2011). Discharge and water temperature values simulated at RM 0.5 on the Trinity River were input as a boundary condition of the Klamath River RBM10 model. Tributary inputs that define boundary conditions were otherwise unchanged, and the historical meteorological data were used. The river geometry of the Klamath River model was truncated to establish Iron Gate Dam as a headwater boundary. Using the historical and prescribed dam releases, we were then able to assess the cold water Trinity River augmentation effects

on lower Klamath River water temperature by comparing the simulated water temperatures at Klamath, California.

For the augmentation scenarios, Reclamation provided three release schedules with specific release-point temperatures for Lewiston Dam and the planned 2015 operational release schedule for Iron Gate Dam on the Klamath River. Water releases from Lewiston Dam were scheduled to achieve flow targets of 2,500, 2,800, and 3,200 ft^3/s in the lower mainstem Klamath River (RM 5.7) near Klamath, California, when combined with tributary flows and the planned 2015 release schedule for Iron Gate Dam. Water temperatures downstream of Iron Gate Dam in 2014 were used as the uppermost boundary condition of the Klamath River model, with the selection based on similarities to 2015 with regard to reservoir management, Iron Gate Dam release schedules, and drought-condition meteorology. The release schedules covered the period of July 20–November 30, with flow targets timed to coincide with the upstream migration of adult fall-run Chinook salmon. We also simulated a baseline referred to as the "No Action" alternative scenario that was based on historical tributary flows, meteorology, and dam releases observed in 1994. Although conditions in 2015 were not exactly the same as in 1994, differing in historical tributary flows, temperatures, and meteorology, alternative scenarios based on 1994 were exactly the same except for dam outflows and temperatures. Thus, temperature difference between targeted flow scenarios and the No Action baseline allowed us to directly assess the effect of each scenario on water temperature in the lower Klamath River in 1994, a year with conditions similar to those of 2015.

Results

Calibration and Validation

Based on measures of precision and bias, we selected the wind function without a seasonal component (eq. 11) for simulating water temperatures of the Trinity River. For every reach, measures of precision (RMSE and MAE) were slightly less for the model with constant evaporation coefficients (table 3) compared to the model with seasonal evaporation coefficients (table 4). Furthermore, bias (as measured by the mean error) was smaller for the model with constant evaporation coefficients (table 3) than for the model with seasonal evaporation coefficients (table 4). For the model with constant evaporation coefficients, the residuals as a function of water temperature indicated little bias for reaches 1–4, a slight negative bias at low water temperature for reaches 4–8, and a slight positive bias at high water temperature for reaches 7 and 8 (figs. 8 and 9). We used the wind function with constant evaporation coefficients for all subsequent water temperature simulations (table 3).

Overall, RBM10 performed well in simulating water temperatures of the Trinity River. Simulated water temperature tracked observed temperature closely, capturing both seasonal and short-term fluctuations in observed water temperatures (figs. 10 and 11). Therefore, precision for each model reach was favorable. The RMSE ranged from 0.25 to 1.12 °C and MAE ranged from 0.18 to 0.89 °C among locations (table 3, figs. 8 and 9).

Table 3. Best-fit parameter estimates of the wind function shown in equation 11 and goodness-of-fit statistics for observed and simulated water temperatures at eight locations along the Trinity River.

[Statistics are defined as follows: *n*, sample size; NSS, Nash-Sutcliffe statistic; RMSE, root mean square error; ME, mean error (mean of simulated-measured); MAE, mean absolute error]

Meteorological reach	Location (river mile)	$\hat{a}_r$	$\hat{b}_r$	$\hat{\theta}_r$	*n*	NSS	RMSE	ME	MAE
1	107.7	2.59E-09	2.19E-09	12.213	3,464	0.974	0.250	-0.013	0.178
2	79.2	1.68E-10	8.07E-14	0.408	3,205	0.963	0.704	-0.172	0.550
3	58.6	3.58E-13	5.21E-12	1.570	3,270	0.972	0.790	-0.160	0.608
4	47.5	5.11E-10	4.58E-14	0.781	3,276	0.965	0.951	-0.289	0.742
5	31.5	6.35E-10	2.06E-11	0.581	3,036	0.955	1.119	-0.511	0.887
6	21.2	2.16E-11	4.61E-11	1.747	1,877	0.965	0.954	-0.160	0.701
7	12.5	5.51E-11	3.31E-10	0.999	2,225	0.972	0.914	-0.310	0.729
8	0.5	1.33E-10	2.02E-10	2.508	3,212	0.967	1.025	-0.437	0.821

Table 4. Best-fit parameter estimates of the wind function shown in equation 12 and goodness-of-fit statistics for observed and simulated water temperatures at eight locations along the Trinity River.

[Statistics are defined as follows: *n*, number of days with observed water-temperature data; NSS, Nash-Sutcliffe statistic; RMSE, root mean square error; ME, mean error (mean of simulated-observed); MAE, mean absolute error]

Meteorological reach	Location (river mile)	$\hat{a}_{r,1}$	$\hat{b}_{r,1}$	$\hat{a}_{r,2}$	$\hat{b}_{r,2}$	$\hat{\theta}_r$	*n*	NSS	RMSE	ME	MAE
1	107.7	1.70E-08	4.68E-10	7.40E-09	1.78E-09	12.177	3,464	0.974	0.251	-0.028	0.176
2	79.2	3.57E-12	4.48E-13	1.01E-09	3.18E-13	0.398	3,205	0.961	0.721	-0.177	0.567
3	58.6	7.67E-11	1.71E-12	8.16E-10	5.45E-11	1.782	3,270	0.971	0.804	-0.225	0.618
4	47.5	1.56E-09	1.99E-11	3.04E-13	8.49E-12	0.645	3,276	0.960	1.013	-0.405	0.793
5	31.5	4.00E-10	4.19E-12	7.00E-10	9.15E-11	0.559	3,036	0.952	1.146	-0.520	0.908
6	21.2	9.53E-11	2.25E-11	4.19E-09	8.28E-10	4.430	1,877	0.963	0.973	-0.256	0.713
7	12.5	2.72E-11	7.46E-12	8.30E-09	6.80E-09	3.729	2,225	0.967	0.995	-0.531	0.801
8	0.5	3.97E-10	2.23E-10	2.81E-11	6.08E-11	0.890	3,212	0.964	1.074	-0.472	0.864

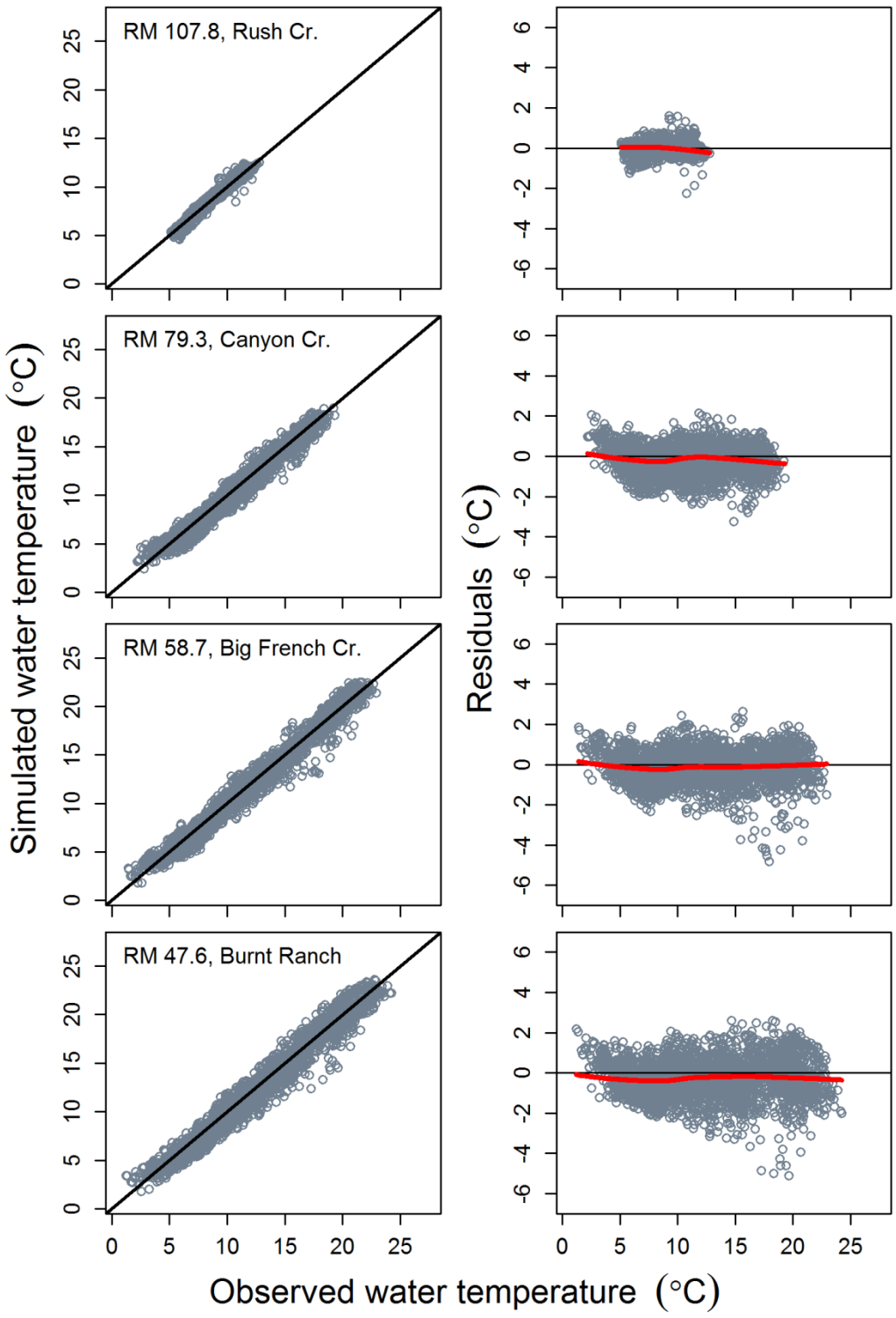

Figure 8. Graphs showing simulated water temperature and residuals (simulated minus observed temperature) as a function of observed water temperature at five locations between river miles (RMs) 107.8 and 47.6 of the Trinity River. Red lines in the four graphs in the right column show a LOWESS smoother (locally weighted polynomial regression) to indicate trend in residuals.

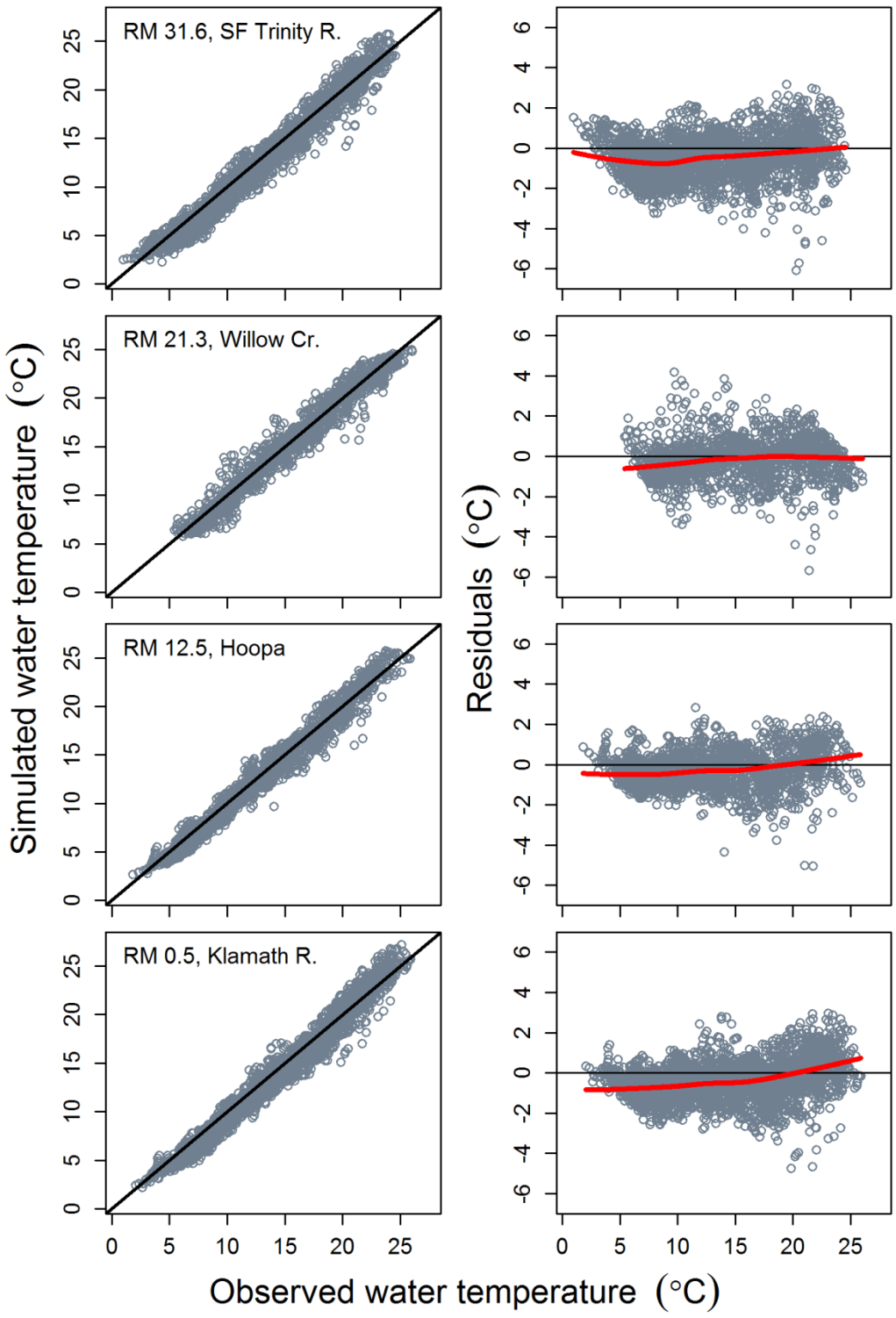

Figure 9. Graphs showing simulated water temperature and residuals (simulated minus observed temperature) as a function of observed water temperature at four locations between river miles (RMs) 31.6 and 0.5 of the Trinity River. Red lines show a LOWESS smoother (locally weighted polynomial regression) to indicate trend in residuals.

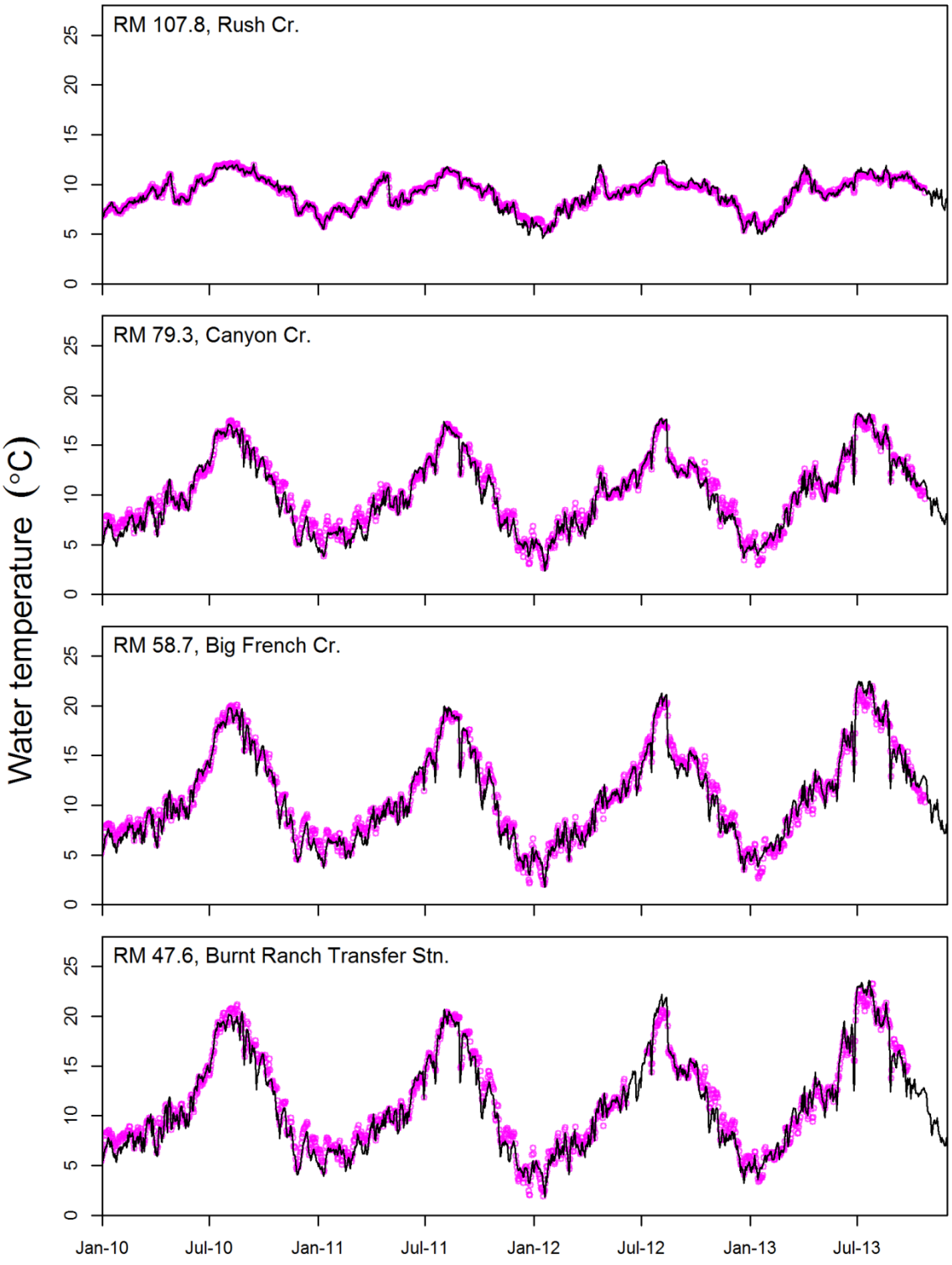

Figure 10. Time series of simulated (solid line) and observed water temperature (o) at river miles 107.8, 79.3, 58.7, and 47.6, Trinity River, 2010–2013. Water temperature was simulated using best-fit coefficients from model calibration. Complete 34-year time series is shown in figures A1–A4.

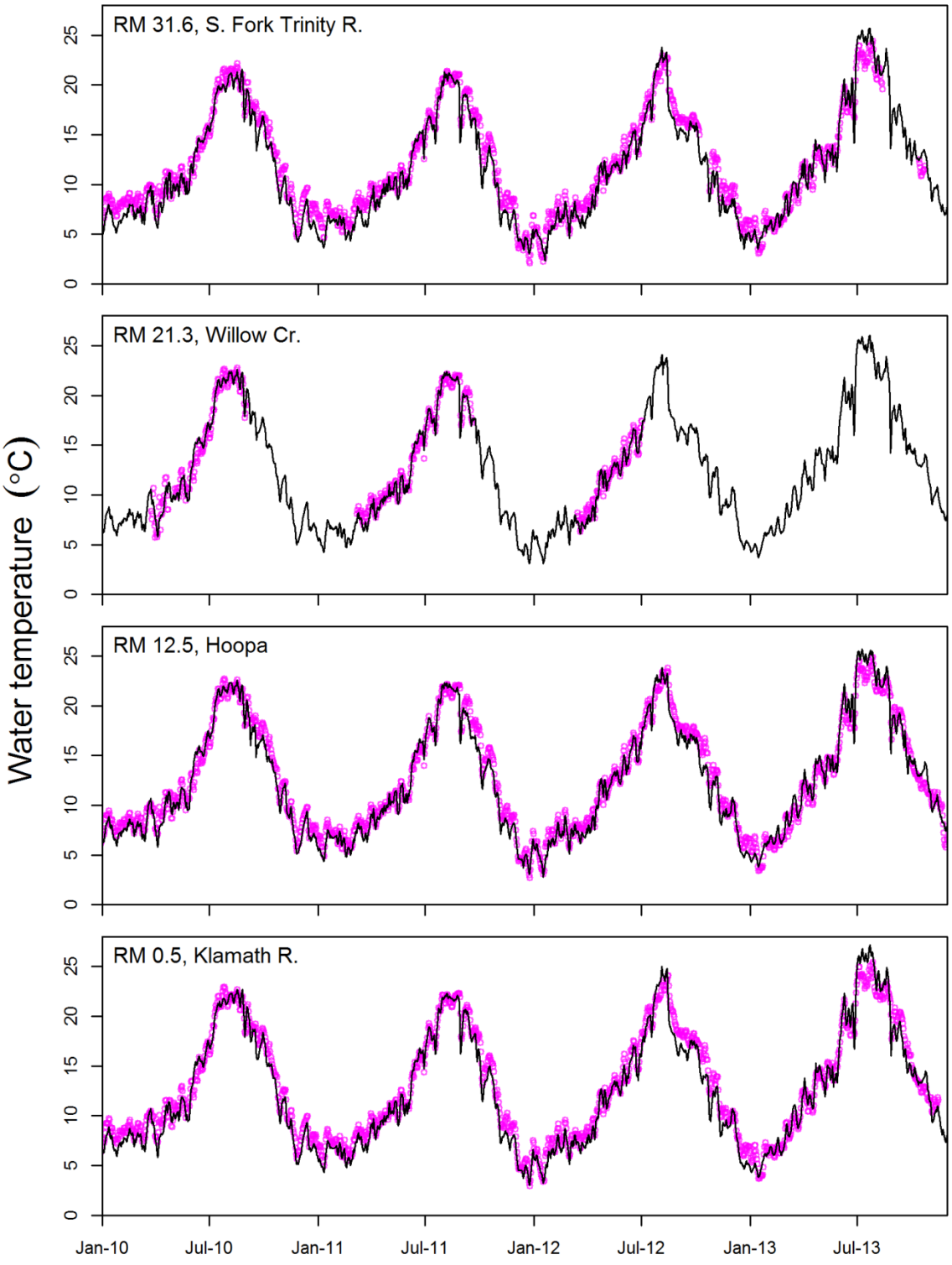

Figure 11. Time series of simulated (solid line) and observed water temperature (o) at river miles 31.6, 21.3, 12.5, and 0.5, Trinity River, 2010–2013. Water temperature was simulated using best-fit coefficients from model calibration. Complete 34-year time series is shown in figures A5–A8.

Although the calibrated model fit the observed data well, it is important to consider performance when the model is used to simulate water temperatures that are outside the range of data used to calibrate the model. Our cross-validation analysis indicated that the model performed well when compared with observed data excluded from the calibration process (table 5, figs. 12 and 13). Aggregate estimates of prediction error from the cross-validation were nearly equal (table 5) to goodness-of-fit statistics from the calibration (table 3). If the parameter estimates had depended strongly on a particular year of observed data, the prediction error may have been considerably larger than indicated by the calibration statistics. We attribute the favorable prediction error to the structure of RBM10 and the extensive set of observed water temperature data used to inform the model. With such a dataset, excluding any given year from the calibration has a minor effect on the parameter estimates and subsequent simulations (table A3).

On average across the 34-year historical time series, the mean of daily mean water temperature ranged from about 7 °C in early January to 11 °C in late July at Lewiston Dam and from 5 to 23 °C at Hoopa, California (fig. 14). The 2.5th and 97.5th percentiles of daily mean temperature for the historical time series yields a 3 °C interval about the mean at Lewiston Dam and a 6 °C interval at Hoopa, California (fig. 14). The complete time series at each of the calibration sites is shown in figures A1–A8.

Table 5. Aggregate cross-validation estimates of prediction error for evaluating observed and simulated water temperatures at eight locations along the Trinity River.

[The aggregate cross-validation estimates are the weighted averages of the yearly estimates shown in table A3. Statistics are defined as follows: *n*, number of days with observed water-temperature data; NSS, Nash-Sutcliffe statistic; RMSE, root mean square error; ME, mean error; MAE, mean absolute error]

Reach	River mile	Number of years	n	NSS	RMSE	ME	MAE
1	107.8	11	3,464	0.971	0.242	-0.013	0.178
2	79.3	13	3,205	0.952	0.695	-0.172	0.550
3	58.7	13	3,270	0.960	0.783	-0.160	0.608
4	47.6	13	3,276	0.948	0.948	-0.290	0.742
5	31.6	12	3,036	0.938	1.113	-0.511	0.887
6	21.3	11	1,877	0.945	0.931	-0.160	0.701
7	12.5	7	2,225	0.969	0.912	-0.310	0.729
8	0.5	12	3,212	0.957	1.018	-0.437	0.821

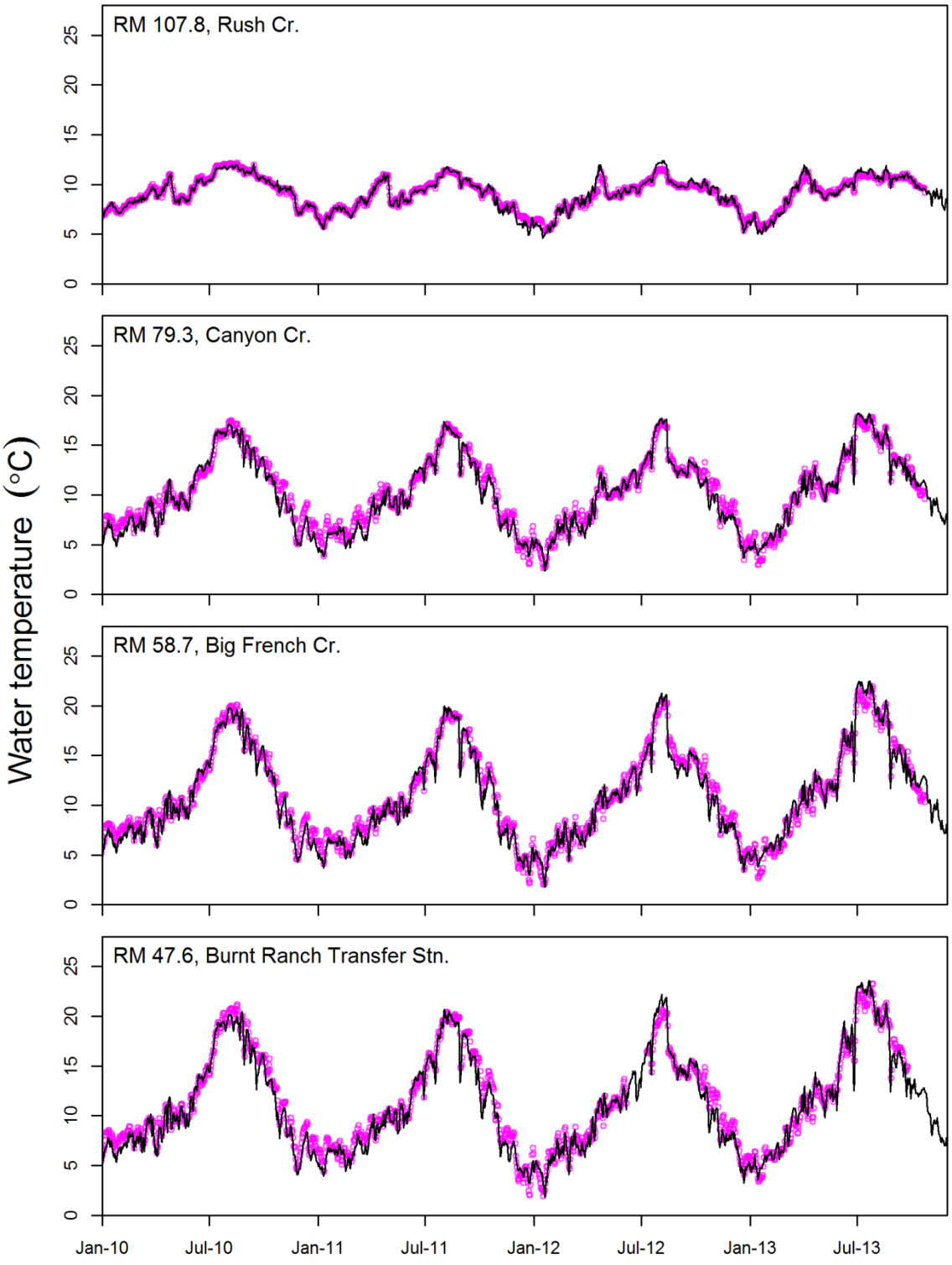

Figure 12. Validation plots showing time series of simulated (solid line) and observed water temperature (o) at river miles 107.8, 79.3, 58.7, and 47.6, Trinity River, 2010–2013. For each year *k*, water temperature was simulated by estimating model coefficients with *k*th year of observed data excluded, and then using those coefficients to simulate water temperature in year *k* (see table A3).

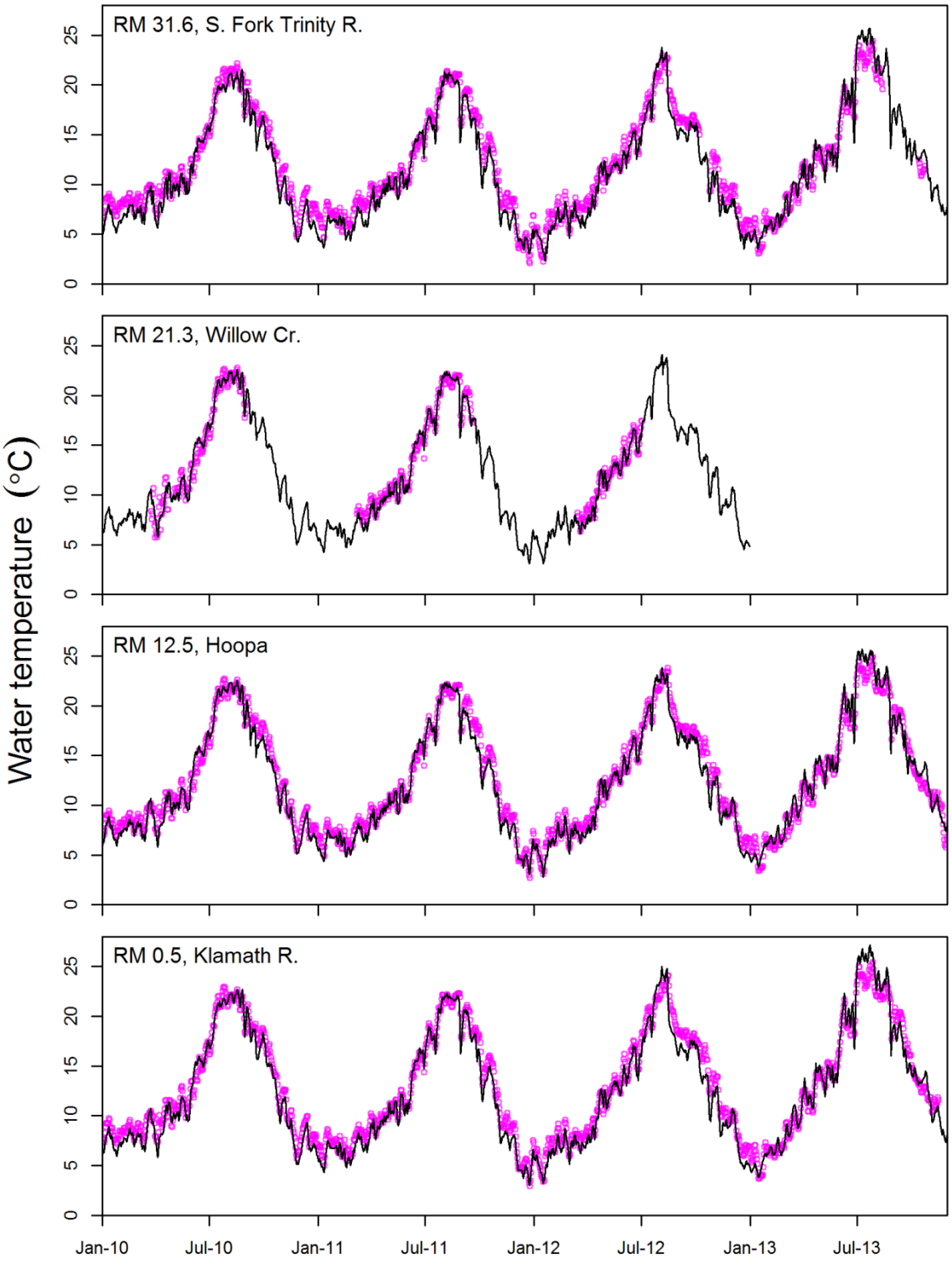

Figure 13. Validation plots showing time series of simulated (solid line) and observed water temperature (o) at river miles 31.6, 21.3, 12.5, and 0.5, Trinity River, 2010–2013. For each year *k*, water temperature was simulated by estimating model coefficients with *k*th year of observed data excluded, and then using those coefficients to simulate water temperature in year *k* (see table A3).

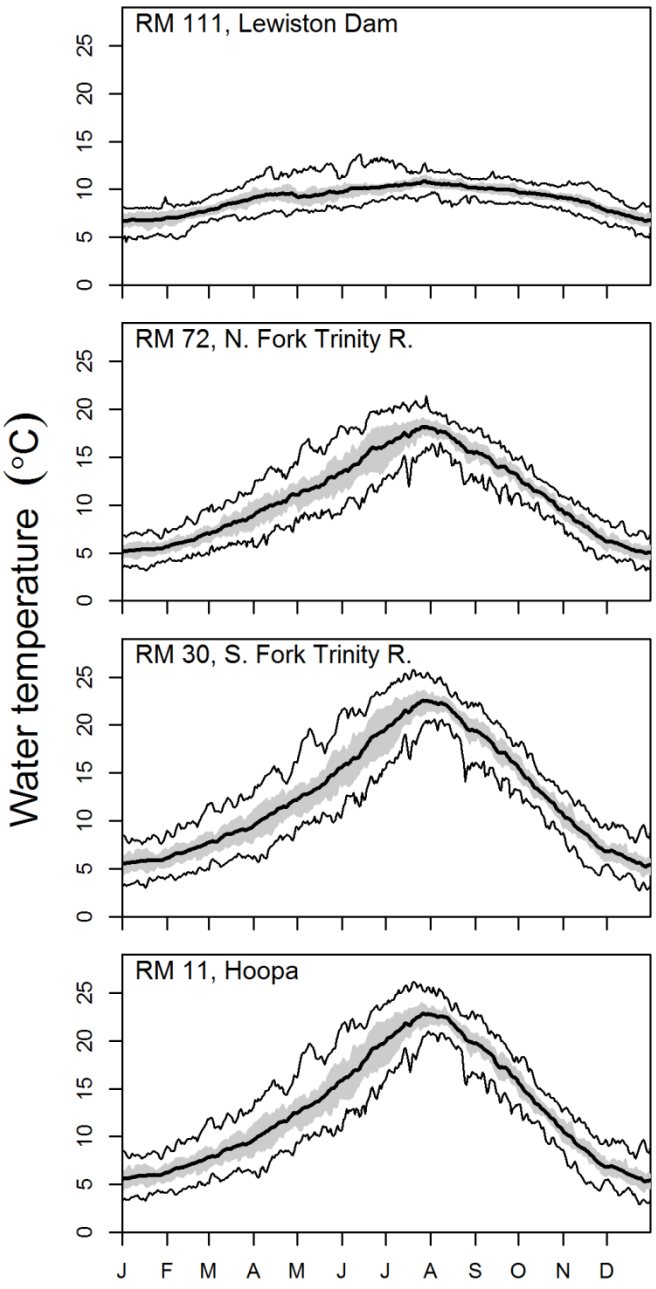

Figure 14. Graphs showing 34-year historical time series of daily mean water temperatures simulated at four locations on the Trinity River, northern California. Thick line shows mean temperature on a given day, shaded area shows the interquartile range (25th–75th percentiles), and thin lines bound 2.5th–97.5th percentiles.

Alternative Management Scenarios

Flow Augmentation Effects on Water Temperature in the Lower Klamath River

We selected the drought year of 1994 to model a historical baseline "No Action" alternative to evaluate the effects of targeted cold water releases at Lewiston Dam on water temperatures in the lower Klamath River. With No Action, the simulated historical daily mean water temperature at RM 5.7 on the lower Klamath River was greater than or near 23 °C for most of August (fig. 15). In mid-August, when flow augmentation through the bypass was ramped up, water temperatures were simulated to decrease to less than the historical baseline under all targeted flow augmentation scenarios (2,500, 2,800, and 3,200 ft^3/s in the lower Klamath River). The three augmentation scenarios uniformly produced an initial 5 °C decrease in daily mean water temperature in response to a short-duration tribal "Boat Dance" pulse flow scheduled as part of the anticipated 2015 operations by Reclamation that was common to all augmentation alternatives. After the initial temperature decrease triggered by the Boat Dance release, an approximate 1 °C difference in water temperature emerged between each of the three augmentation scenarios, with higher targeted flows associated with greater reductions in water temperature. Under each targeted flow scenario, daily mean water temperatures were projected to be less than 21 °C for the duration of the augmentation period. In late September with No Action, lower Klamath River water temperatures decreased to about 21 °C, and a steady decrease in daily mean water temperature commenced as the calendar shifted towards winter. Augmentation was curtailed at that time, and the projected water temperatures for all scenarios converged.

Discussion

Water temperature is a critical water-quality parameter influencing fish populations, as well as the structure of the food webs on which they depend. Understanding how water-management actions in the Trinity River drainage basin affect water temperatures not just in the Trinity River, but also farther downstream in the lower Klamath River, is therefore a critical element in forecasting how such actions will influence salmonid populations of the Klamath Basin. Here, we developed a water-temperature model for the Trinity River capable of simulating daily mean water temperature along the longitudinal gradient of the river from RM 112.2 (Lewiston Dam) to the Klamath River confluence. We calibrated and validated the model to an extensive set of observed water temperatures, allowing us to recreate a 34-year historical record of daily mean water temperature. The model proved useful in comparing the effects of bypass flow augmentation scenarios that targeted flows of 2,500, 2,800, and 3,200 ft^3/s in the lower Klamath River, which were intended to lower water temperatures and decrease risk of disease in adult salmon returns in a drought year. Key findings from these simulations indicated that (1) bypass augmentation can reduce water temperatures in the lower Klamath River by as much as 5 °C, (2) reduction in water temperature is proportional to the augmentation rate, and (3) a flow target as low as 2,500 ft^3/s was likely to keep daily mean water temperatures equal to or less than 21 °C from mid-August to late September, assuming tributary hydrology and metrology in 2015 is consistent with the hydrology and metrology in 1994 used in the simulations. Given that model accuracies are about ±1 °C for both Trinity and Klamath RBM10 models (table 4, figs. 8–9; Perry and others, 2011) and uncertainties and potential differences in tributary inflows and metrology between 1994 and 2015, a flow target of 2,800 ft^3/s would more conservatively ensure that temperatures would remain less than 23 °C.

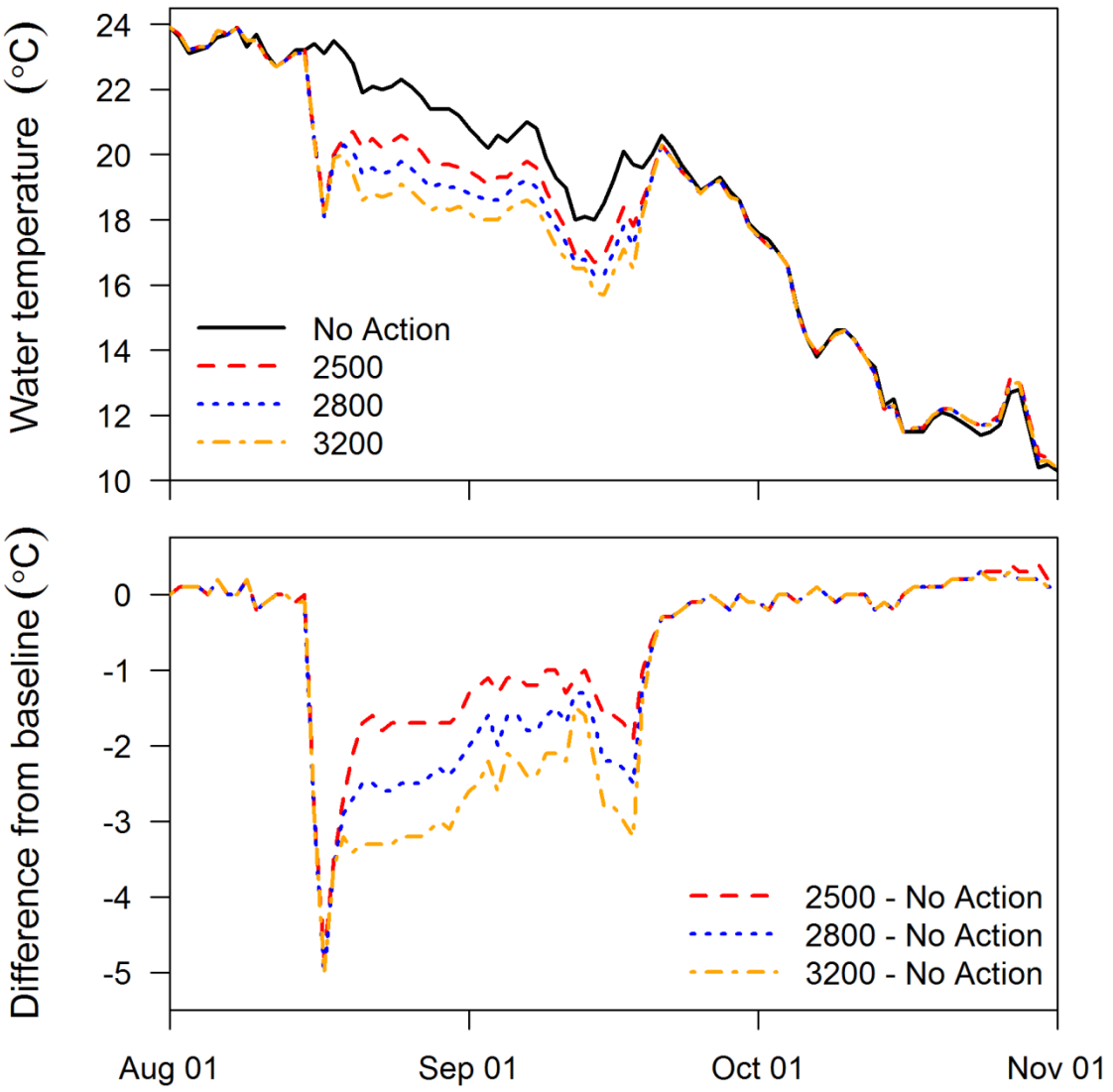

Figure 15. Simulated daily mean water temperatures at river mile 5.7 in the lower Klamath River near Klamath, California, during 1994, under four management scenarios that include targeted flows of 2,500, 2,800, and 3,200 cubic feet per second, augmented by Lewiston Dam bypass, and the historical baseline "No Action" alternative (top). Difference in temperature (targeted flow scenario minus No Action alternative) shows relative effects of bypass augmentation (bottom).

In evaluating the simulated temperature effects of the various management alternatives, temperatures near or exceeding 23 °C are of particular interest, as this has been identified as a threshold for impairing the upstream migration of adult salmon (Strange, 2010a)—a threshold regarded as a "thermal migration barrier." Under the No Action scenario, water temperatures in the lower Klamath River were simulated to approach or exceed 23 °C during most of August (fig. 15). Adult fall-run Chinook salmon (*Oncorhynchus tshawytscha*) typically begin entering the Klamath River in late August, and a thermal migration barrier can cause fish to congregate at high densities in the lower river, particularly in years with below average streamflow. Stream conditions of this type can lead to epizootic outbreaks of *Ichthyophthirius multifiliis* ("Ich") and *Flavobacterium columnare* ("Columnaris"), diseases that were associated with the massive Klamath River fish kill of 2002 (Guillen, 2003a, 2003b; Turek and others, 2004). Although water temperature is an important factor of epizootic outbreaks, other factors such as fish density and streamflow must also be considered (Bodensteiner and others, 2000; Strange, 2010b; U.S. Fish and Wildlife Service and National Oceanographic and Atmospheric Administration, 2013; Belchick, 2015). Nonetheless, the augmentation scenarios we present in this study provide a working example of how the Trinity and Klamath RBM10 models can be used to inform management decisions as needed to protect salmon populations in the Klamath Basin given limited water resources.

As meteorological and streamflow data become available, the Trinity River water-temperature model can easily be updated in the future. The next step is to make available an integrated Trinity/Klamath RBM10 water-temperature model that can be used to directly inform real-time resource management decisions such as the example presented in this report, as well as function as a critical sub model for salmon life-cycle modeling efforts currently underway as an additional decision-support tool for managers.

Temperatures near or greater than 23 ^{o}C may not be common in the lower Trinity River at the time when adult fall-run Chinook salmon begin their annual migration (fig. 14). However, climate change projections suggest higher temperatures will become increasingly common in the future (Perry and others, 2011; Flint and Flint, 2012), which will place additional stressors on adult salmon runs. The Trinity/Klamath RBM10 water-temperature model likely will prove beneficial to further our understanding of the relationship between water temperature and salmon populations of the Klamath Basin, as it will improve ability of managers to make informed water-management decisions during drought-like conditions assumed to increase in frequency as a result of climate change.

Acknowledgments

Construction of this water-temperature model was a significant undertaking and would not be possible without the help of many. Funding was provided by Bureau of Reclamation (Agreement R14PG00145ed) and U.S. Fish and Wildlife Service (Agreement 4500054074). We thank California Department of Water Resources and Watercourse Engineering, Inc., for the river geometry data. Scott Evans of the U.S. Geological Survey processed the river geometry with the Hydrologic Engineering Centers River Analysis System to output the data fundamental to characterizing the hydraulics of the Trinity River. Andrea McBroom with the U.S. Forest Service, Paul Zedonis with the Bureau of Reclamation, Edward Oldenberg with the Hoopa Valley Tribe, and Aaron Martin with the Yurok Tribe all helped gather the extensive water-temperature dataset required to construct and calibrate the model. Ben Livneh provided the gridded wind data. The map of the watershed was artfully created by Mark Hereford of the U.S. Geological Survey. Finally, we must thank Paul Zedonis, again, and Danielle Hereford of the U.S. Geological Survey for their constructive reviews of this report. To the unsung heroes who collected the field data, and others we did not mention, please know we are grateful.

References Cited

Ångström, A., 1918, A study of the radiation of the atmosphere: Smithsonian Institute Miscellaneous Collection, v. 65, p. 159–161.

Belchik, M., 2015, An Outbreak of *Ichthyophthirius multifiliis* in the Klamath and Trinity Rivers in 2014 (draft report): Yurok Tribal Fisheries Program Data Series Report, 56 p.

Benjamin, J.R., Connolly, P.J., Romine, J.G., and Perry, R.W., 2013, Potential effects of changes in temperature and food resources on life history trajectories of juvenile *Oncorhynchus mykiss*: Transactions of the American Fisheries Society, v. 142, no. 1, p. 208–220.

Bodensteiner, L.R., Sheehan, R.J., and Wills, P.S., 2000, Flowing water—An effective treatment for *Ichthyophthiriasis*: Journal of Aquatic Animal Health, v. 12, no. 3, p. 209–219.

California Department of Water Resources, 2014, Trinity River flood insurance study hydraulic analysis—Technical summary, March 2014: California Department of Water Resources, Northern Region Office, Cooperating Technical Partners, grant nos. EMF-2008-GR-0808 and EMF-2011-GR-1109, 12 p.

Davison, A.C., and Hinkley, D.V., 1997, Bootstrap methods and their application—Cambridge series in statistical and probabilistic mathematics (1st ed.): Cambridge, United Kingdom, Cambridge University Press, 592 p.

Deas, M.L., 1998, Trinity Reservoir water temperature simulation model: Prepared for Trinity County Planning Department, Natural Resources Division, August 1998, 27 p.

Deas, M.L. 2002, Trinity Reservoir inflow temperature monitoring study: Prepared for Trinity County Planning Department, June 2002.

Deas, M.L., and Orlob, G.T., 1999, Klamath River modeling project: Davis, University of California, report no. 99-04, 235 p. + appendixes.

Edinger, J.E., Brady, D.K., and Geyer, J.C., 1974, Heat exchange and transport in the environment: Electric Power Research Institute, Cooling Water Discharge Research Project, RP-49, 125 p.

Flerchinger, G.N., Xaio, W., Marks, D., Sauer, T.J., and Qiang, Y., 2009, Comparison of algorithms for incoming atmospheric long-wave radiation: Water Resources Research, v. 45, no. 3, 13 p.

Flint, L.E., and Flint, A.L., 2008, A basin-scale approach to estimating stream temperatures of tributaries to the Lower Klamath River, California: Journal of Environmental Quality, v. 37, 68 p.

Flint, L.E., and Flint, A.L., 2012, Estimation of stream temperature in support of fish production modeling under future climates in the Klamath River Basin: U.S. Geological Survey Scientific Investigations Report 2011–5171, 31 p.

Guillen, G., 2003a, Klamath River fish die-off September 2002, Causative factors of mortality: U.S. Fish and Wildlife Service, Arcata Fish and Wildlife Office, Arcata, California, report no. AFWO-F-02-03, 115 p.

Guillen, G., 2003b, Klamath River fish die-off September 2002, Report on estimate of mortality: U.S. Fish and Wildlife Service, Arcata Fish and Wildlife Office, Arcata, California, report no. AFWO-01-03, 28 p.

Henderson-Sellers, B., 1986, Calculating the surface energy balance for lake and reservoir modeling—A review: Reviews of Geophysics, v. 24, no. 3, p. 625–649.

Livneh B., Pierce, D.S., Bohn, T.J., Munoz-Ariola, F., Nijssen, B., Cayan, D., Vose, R., and Brekki, L.D., 2015, A spatially comprehensive, hydrometeorological data set for Mexico, the U.S., and Southern Canada 1950–2013: Nature Scientific Data, article no. 150042, 12 p.

Mohseni, Omid, Stefan, H.G., and Erickson, T.R., 1998, A nonlinear regression model for weekly stream temperatures: Water Resources Research, v. 34, no. 10, p. 2,685–2,692.

Perry, R.W., Plum, J.M., Fielding, S.D., Adams, N.S., and Rondorf, D.W., 2013, Comparing effects of transmitters within and among populations—Application to swimming performance of juvenile Chinook salmon: Transactions of the American Fisheries Society, v. 142, no. 4, p. 901–911.

Perry, R.W., Risley, J.C., Brewer, S.J., Jones, E.C., and Rondorf, D.W., 2011, Simulating daily water temperatures of the Klamath River under dam removal and climate change scenarios: U.S. Geological Survey Open-File Report 2011–1243, 78 p.

Perry, R.W., Romine, J.G., Adams, N.S., Blake, A.R., Burau, J.R., Johnston, S.V., and Liedtke, T.L., 2012, Using a non-physical behavioural barrier to alter migration routing of juvenile Chinook salmon in the Sacramento-San Joaquin River Delta: River Research and Applications, v. 30, no. 2, p. 192–203.

Perry, R.W., Skalski, J.R., Brandes, P.L., Sandstrom, P.T., Klimley, A.P., Ammann, A., and MacFarlane. B., 2010, Estimating survival and migration route probabilities of juvenile Chinook salmon in the Sacramento-San Joaquin River Delta: North American Journal of Fisheries Management, v. 30, no. 1, p. 142–156.

Plumb, J.M., Connor, W.P., Tiffan, K.F., Moffitt, C.M., Perry, R.W., and Adams, N.S., 2012, Estimating and predicting collection probability of fish at dams using multistate modeling: Transactions of the American Fisheries Society, v. 141, no. 5, p. 1,364–1,373.

R Core Team, 2014, R: A language and environment for statistical computing: Vienna, Austria, R Foundation for Statistical Computing, *http://www.R-project.org/*.

Strange, J.S., 2010a, Upper thermal limits to migration in adult Chinook salmon—Evidence from the Klamath River Basin: Transactions of the American Fisheries Society, v. 139, no. 4, p. 1,091–1,108.

Strange, J.S., 2010b, Summary of scientific evidence to guide special flow releases to reduce the risk of adult fall Chinook salmon mass disease mortality in the lower Klamath River: Yurok Tribal Fisheries Program, accessed February 24, 2016, at *www.trrp.net*.

Thornton, P.E., Hasenauer, H., and White, M.A., 2000, Simultaneous estimation of daily solar radiation and humidity from observed temperature and precipitation—An application over complex terrain in Austria: Agricultural and Forest Meteorology, v. 104, p. 255–271, http://dx.doi.org/10.1016/S0168-1923(00)00170-2.

Thornton, P.E., and Running, S.W., 1999, An improved algorithm for estimating incident daily solar radiation from measurements of temperature, humidity, and precipitation: Agriculture and Forest Meteorology, v. 93, p. 211–228, http://dx.doi.org/10.1016/S0168-1923(98)00126-9.

Thornton, P.E., Running, S.W., and White, M.A., 1997, Generating surfaces of daily meteorological variables over large regions of complex terrain: Journal of Hydrology, v. 190, p. 214–251, http://dx.doi.org/10.1016/S0022-1694(96)03128-9.

Thornton, P.E., Thornton, M.M., Mayer, B.W., Wilhelmi, N., Wei, Y., Devarakonda, R., and Cook, R.B., 2014, Daymet—Daily surface weather data on a 1-km grid for North America, version 2 data set, spatial range: N=41.14, S=40.65, E=-122.86, W=-123.69, temporal range—1980/01/01–2014/12/31: Oak Ridge, Tennessee, Oak Ridge National Laboratory Distributed Active Archive Center, accessed July 29, 2015, at http://daac.ornl.gov.

Turek, S., Rode, M., Cox, B., Heise, G., Sinnen, W., Reese, C., Borok, S., Hampton, M., and Chun, C., 2004, September 2002 Klamath River fish-kill—Final analysis of contributing factors and impacts: California Department of Fish and Game, 183 p.

Unsworth, M.H., and Monteith, J.L., 1975, Long-wave radiation at the ground—I, Angular distribution of the incoming radiation: Quarterly Journal of the Royal Meteorological Society, v. 101, p. 13–24.

U.S. Army Corps of Engineers, 2010, HEC-RAS—River analysis system, user's manual version 4.1, January 2010, CPD-68: U.S. Army Corps of Engineers, Institute for Water Resources, Hydrological Engineering Center, 790 p., accessed Sept. 13, 2011, at www.hec.usace.army.mil.

U.S. Fish and Wildlife Service and National Oceanic and Atmospheric Administration, 2013, 2013 Fall flow release recommendation: U.S. Fish and Wildlife Service and National Oceanic and Atmospheric Administration, Memorandum from Irma Lagomarsino and Nicholas Hetrick to Brian Person, Reclamation Northern California Area Manager, 46 p.

Watercourse Engineering, Inc., 2007, Trinity River flow and temperature modeling project: Prepared for Trinity County Planning Department Natural Resources Division and the Trinity River Restoration Program, 172 p.

Western Regional Climate Center, 2015, RAWS USA Climate Archive: Reno, Nevada, Western Regional Climate Center Web site, accessed May 21, 2015, at *http://www.raws.dri.edu*.

Yearsley, J., 2003, Developing a temperature total maximum daily load for the Columbia and Snake Rivers, simulation methods: U. S. Environmental Protection Agency, Region 10, Seattle, Washington, Report 901-R-03-003, 30 p.

Yearsley, J., 2009, A semi-Lagrangian water temperature model for advection-dominated river systems: Water Resources Research, v. 45, 19 p.

Yearsley, J., Karna, D., Peene, S., and Watson, B., 2001, Application of a 1-D heat budget model to the Columbia River system: U.S. Environmental Protection Agency, Region 10, Seattle, Washington, Report 901-R-01-001, 65 p.

Zedonis, Paul, 1997, A water temperature model of the Trinity River: U. S. Fish and Wildlife Service, Arcata, California, 97 p.

Appendix A. River Geometry, Time Series and Water Temperatures, and Prediction Error, Trinity River, Northern California

Table A1. River geometry used in RBM10 for the Trinity River including the estimated *a* and *b* parameters of the continuity equations used to describe the hydraulic properties of the river.

Segment description	Start mile	End mile	Meteorological reach	a_A	b_A	a_W	b_W	Tributary name	River mile
Lewiston Dam to Rush Cr.	112.2	107.7	1	5.366	0.624	16.859	0.322	--	--
Rush Cr. to Grass Valley Cr.	107.7	104.0	1	2.902	0.683	8.666	0.402	Rush Cr.	107.6
Grass Valley Cr. to Steel Bridge	104.0	99.0	1	5.958	0.592	19.464	0.276	Grass Valley Cr.	103.9
Steel Bridge to Indian Cr.	99.0	95.4	1	3.530	0.670	11.382	0.346	--	--
Indian Cr. to Weaver Cr.	95.4	93.9	1	2.360	0.707	18.440	0.291	Indian Cr.	95.2
Weaver Cr. to Douglas City	93.9	92.8	2	3.911	0.631	10.993	0.324	Weaver Cr.	93.8
Douglas City to Reading Cr.	92.8	92.6	2	3.911	0.631	10.993	0.324	Reading Cr.	92.7
Douglas City to Browns Cr.	92.6	87.8	2	3.483	0.654	11.568	0.318	--	--
Browns Cr. to Soldier Cr.	87.8	83.8	2	3.376	0.664	8.139	0.361	Browns Cr.	87.7
Soldier Cr. to Canyon Cr.	83.8	79.2	2	2.264	0.711	4.325	0.468	--	--
Canyon Cr. to Coopers Bar	79.2	75.0	3	1.814	0.733	4.673	0.460	Canyon Cr.	79.1
Coopers Bar to N. Fork Trinity R.	75.0	72.6	3	2.158	0.718	9.334	0.357	--	--
NF Trinity to Eagle Cr.	72.6	69.6	3	3.247	0.677	19.454	0.247	N. Fork Trinity R.	72.5
Eagle Cr. to Price Cr.	69.6	64.0	3	3.457	0.659	43.641	0.161	--	--
Price Cr. to Big French Cr.	64.0	58.6	3	4.206	0.647	29.855	0.195	--	--
Big French Cr. to Italian Cr.	58.6	53.8	4	3.460	0.696	25.038	0.227	Big French Cr.	58.5
Italian Cr. to Burnt Ranch	53.8	48.7	4	5.374	0.633	34.309	0.184	--	--
Burnt Ranch to Transfer Stn.	48.7	47.5	4	3.614	0.688	33.147	0.194	--	--
Transfer Stn. to Burnt Ranch Falls	47.5	44.9	5	1.803	0.686	15.753	0.216	--	--
Burnt Ranch Falls to New R.	44.9	43.7	5	2.339	0.642	63.372	0.069	--	--
New R. to Icebox Cr.	43.7	39.2	5	3.702	0.631	44.572	0.128	New R.	43.6
Icebox Cr. to Quinby Cr.	39.2	34.7	5	6.976	0.644	32.334	0.208	--	--
Quinby Cr. to S. Fork Trinity R.	34.7	31.5	5	3.777	0.690	20.900	0.237	--	--
S. Fork Trinity R. to China Cr.	31.5	28.2	6	11.355	0.630	34.812	0.225	S. Fork Trinity R.	31.3
China Cr. to Willow Cr.	28.2	25.0	6	8.964	0.609	33.569	0.210	--	--
Willow Cr. to W.C. Screw Trap	25.0	21.2	6	2.988	0.695	40.771	0.185	Willow Cr.	24.9

Segment description	Start mile	End mile	Meteorological reach	a_A	b_A	a_W	b_W	Tributary name	River mile
W.C. Screw Trap to Horse Linto Cr.	21.2	19.7	7	10.203	0.599	41.079	0.182	--	--
Horse Linto Cr. to Tish Tang Cr.	19.7	16.4	7	3.314	0.666	40.864	0.166	Horse Linto Cr.	19.6
Tish Tang Cr. to Hoopa	16.4	12.4	7	3.698	0.676	29.703	0.213	Tish Tang Cr.	16.3
Hoopa to Mill Cr.	12.4	8.6	8	3.278	0.714	61.678	0.160	--	--
Mill Cr. to Norton Cr.	8.6	3.9	8	14.600	0.584	54.780	0.158	--	--
Norton Cr. to Klamath R.	3.9	0.0	8	4.879	0.636	69.348	0.109	--	--

Table A2. Midpoint coordinates of the eight meteorological reaches used to extract gridded data.

Reach	Latitude	Longitude	Reach length (miles)
1	40.6939	-122.8605	18.3
2	40.6453	-122.9567	14.7
3	40.7702	-123.1276	20.6
4	40.7889	-123.4389	11.1
5	40.8743	-123.5300	16.0
6	40.9444	-123.6317	10.3
7	41.0256	-123.6407	8.8
8	41.1386	-123.6857	12.4

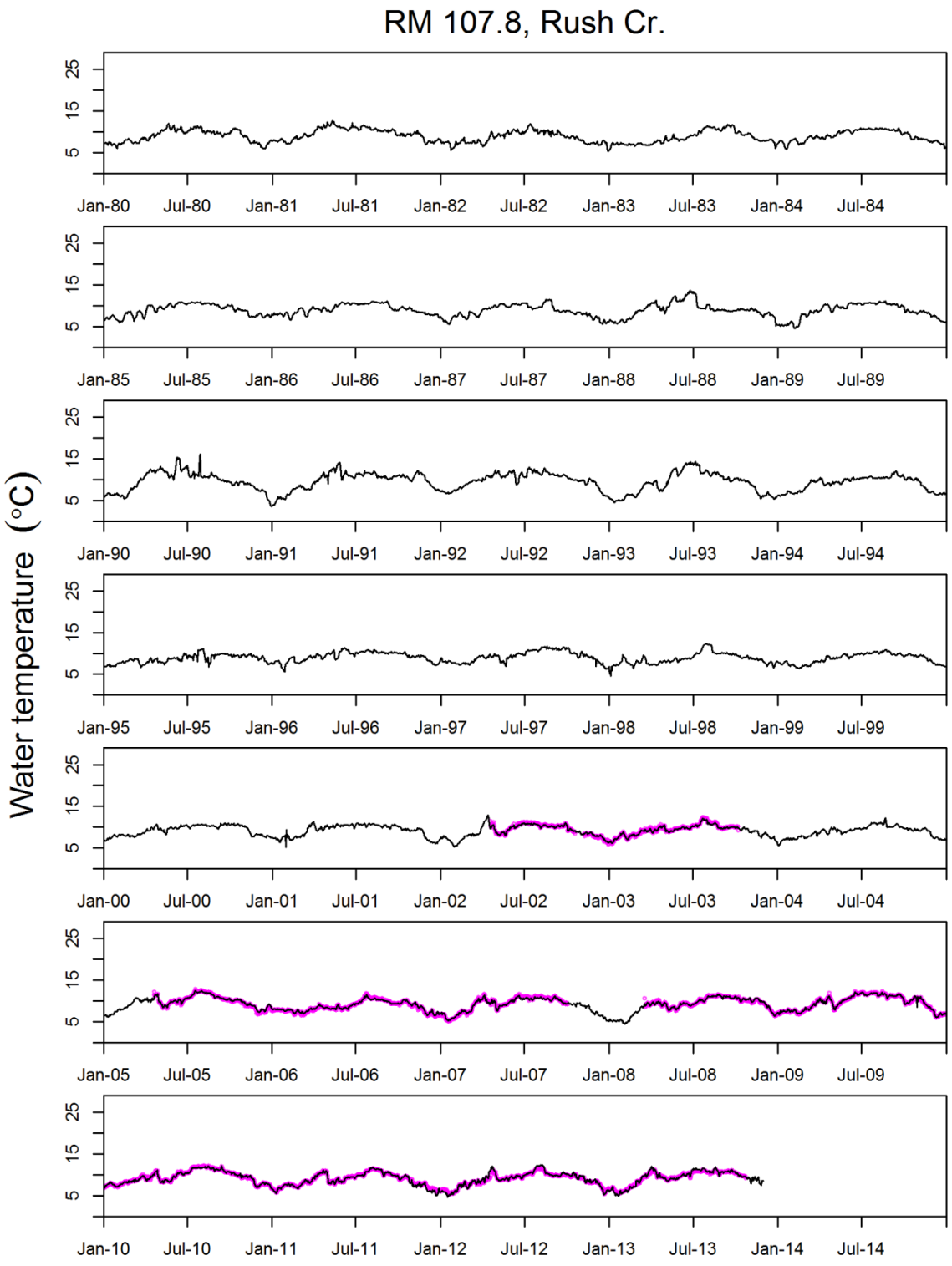

Figure A1. Time series of simulated (solid line) and observed water temperature (o) of the Trinity River at river mile 107.8 near Rush Creek.

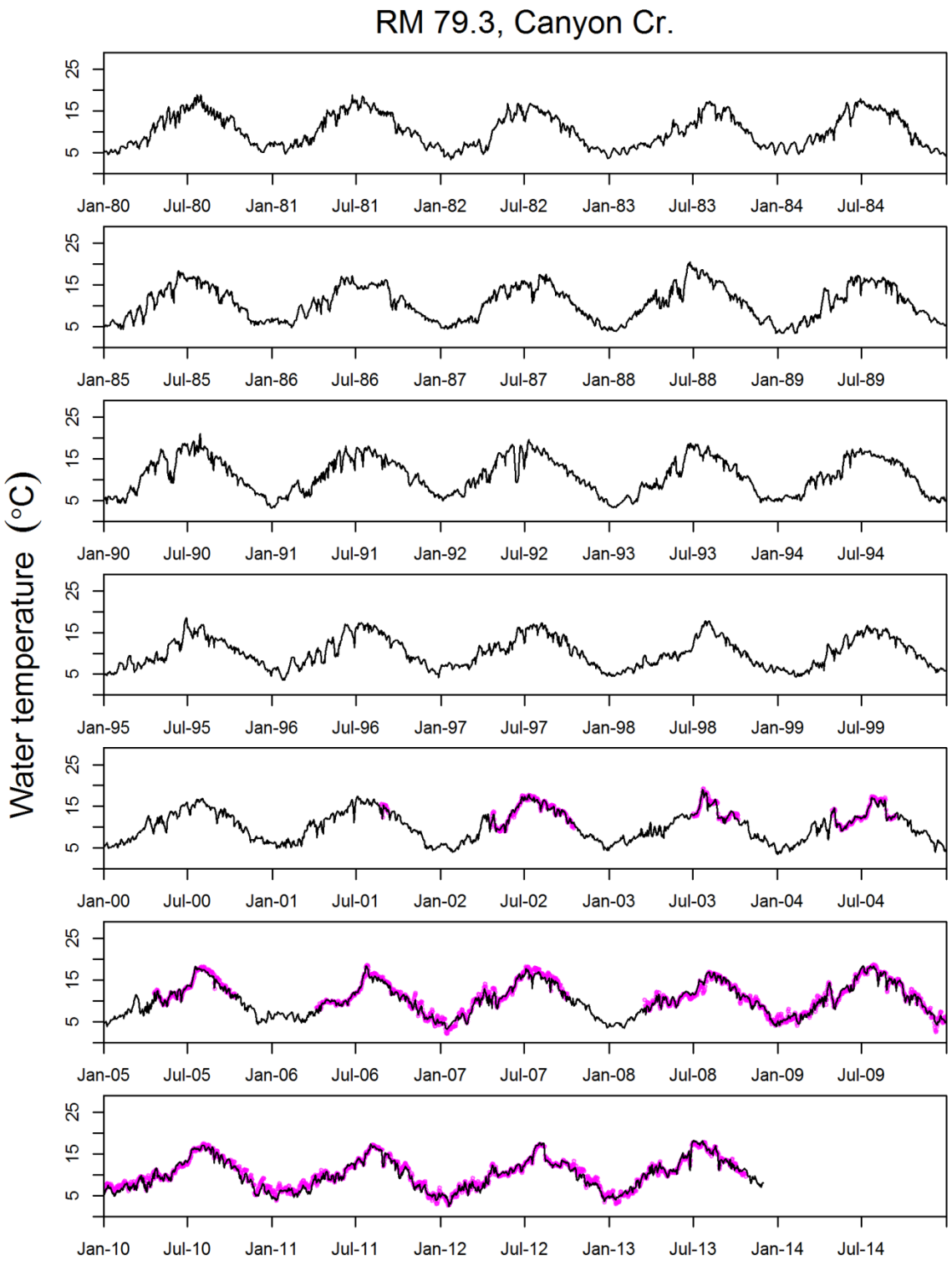

Figure A2. Time series of simulated (solid line) and observed water temperature (o) at river mile 79.3 near Canyon Creek.

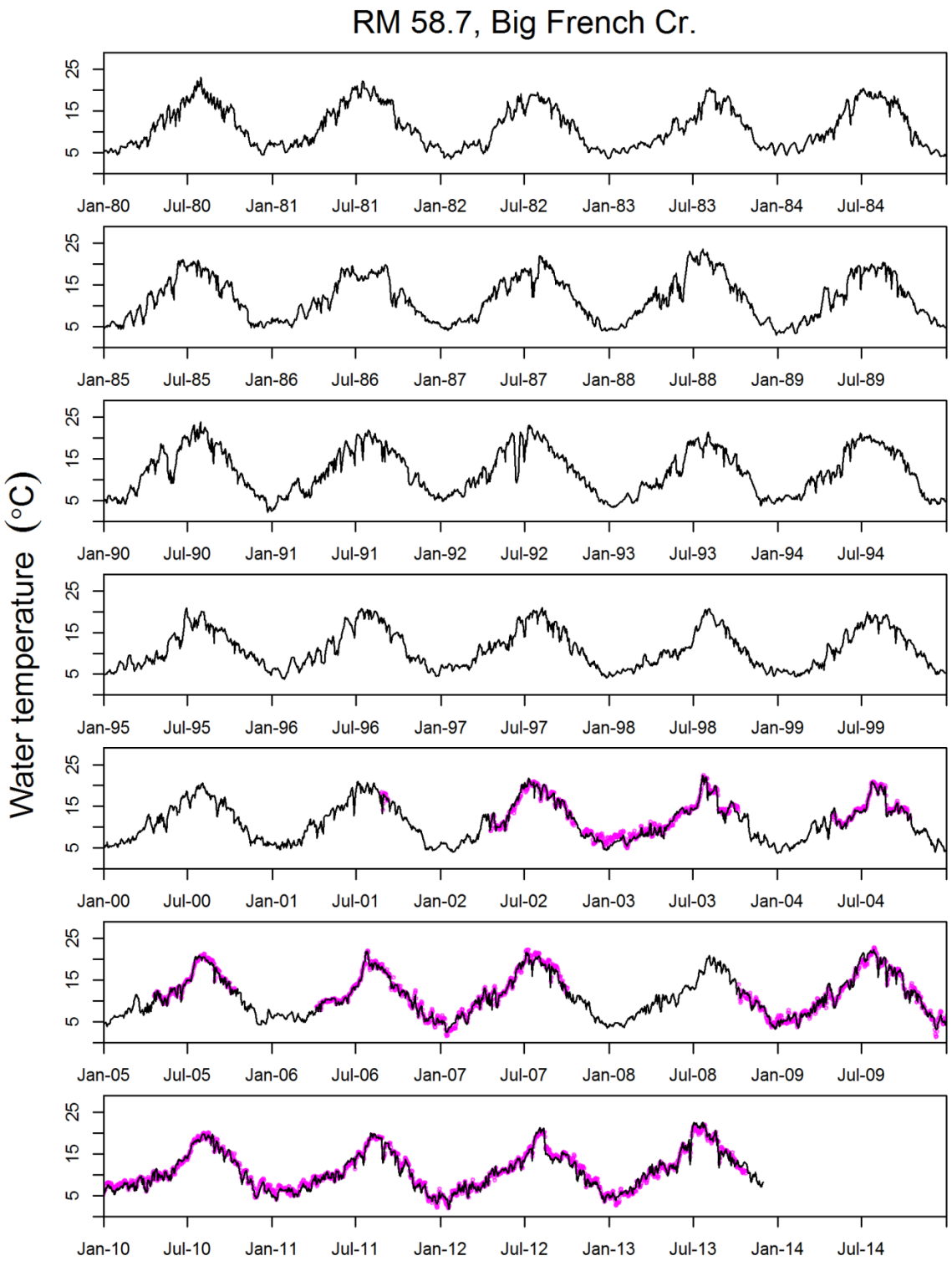

Figure A3. Time series of simulated (solid line) and observed water temperature (o) of the Trinity River at river mile 58.7 near Big French Creek.

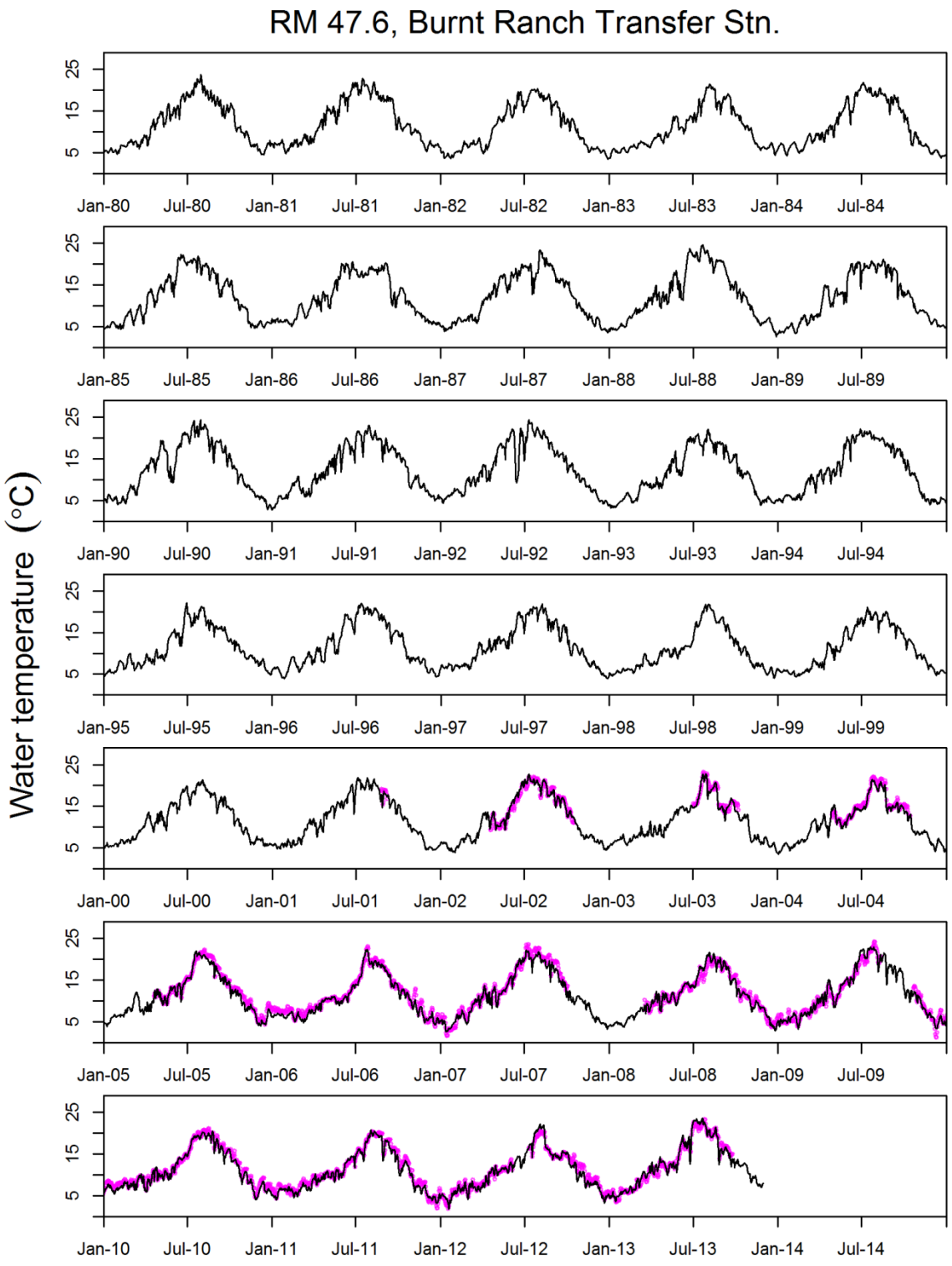

Figure A4. Time series of simulated (solid line) and observed water temperature (o) of the Trinity River at river mile 47.6 near the Burnt Ranch Transfer Station.

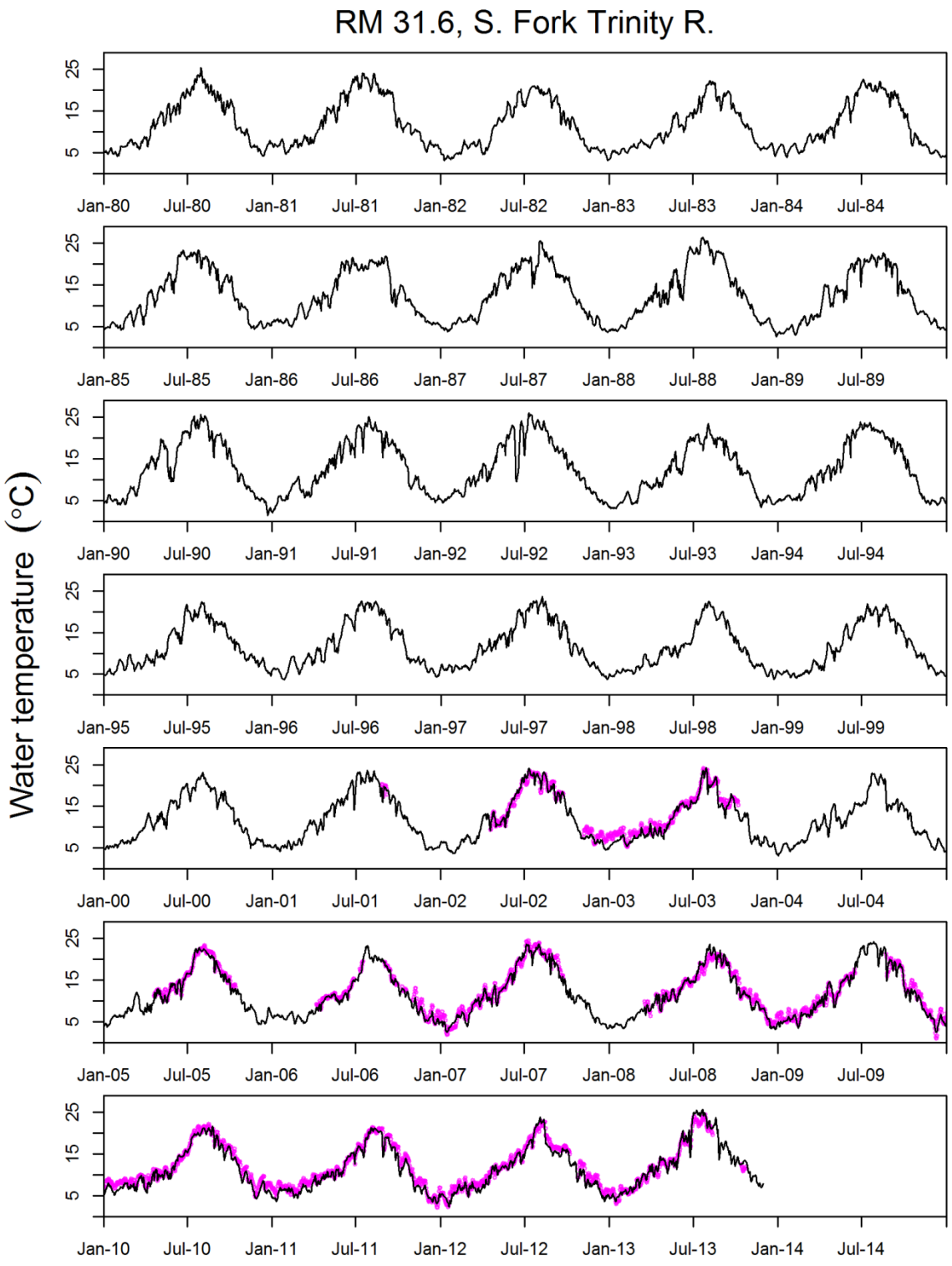

Figure A5. Time series of simulated (solid line) and observed water temperature (o) of the Trinity River at river mile 31.6 near South Fork Trinity River.

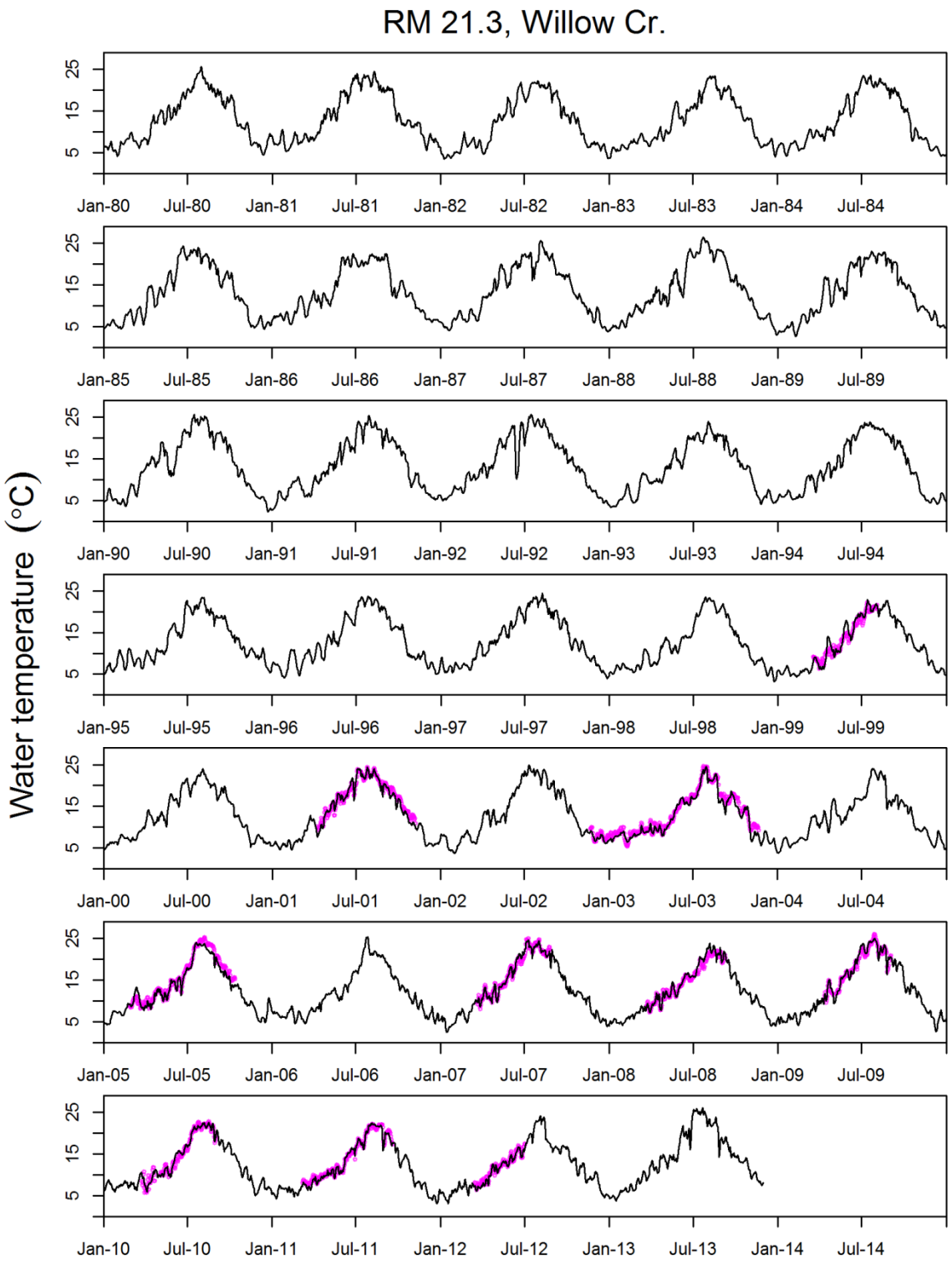

Figure A6. Time series of simulated (solid line) and observed water temperature (o) of the Trinity River at river mile 21.3 near Willow Creek.

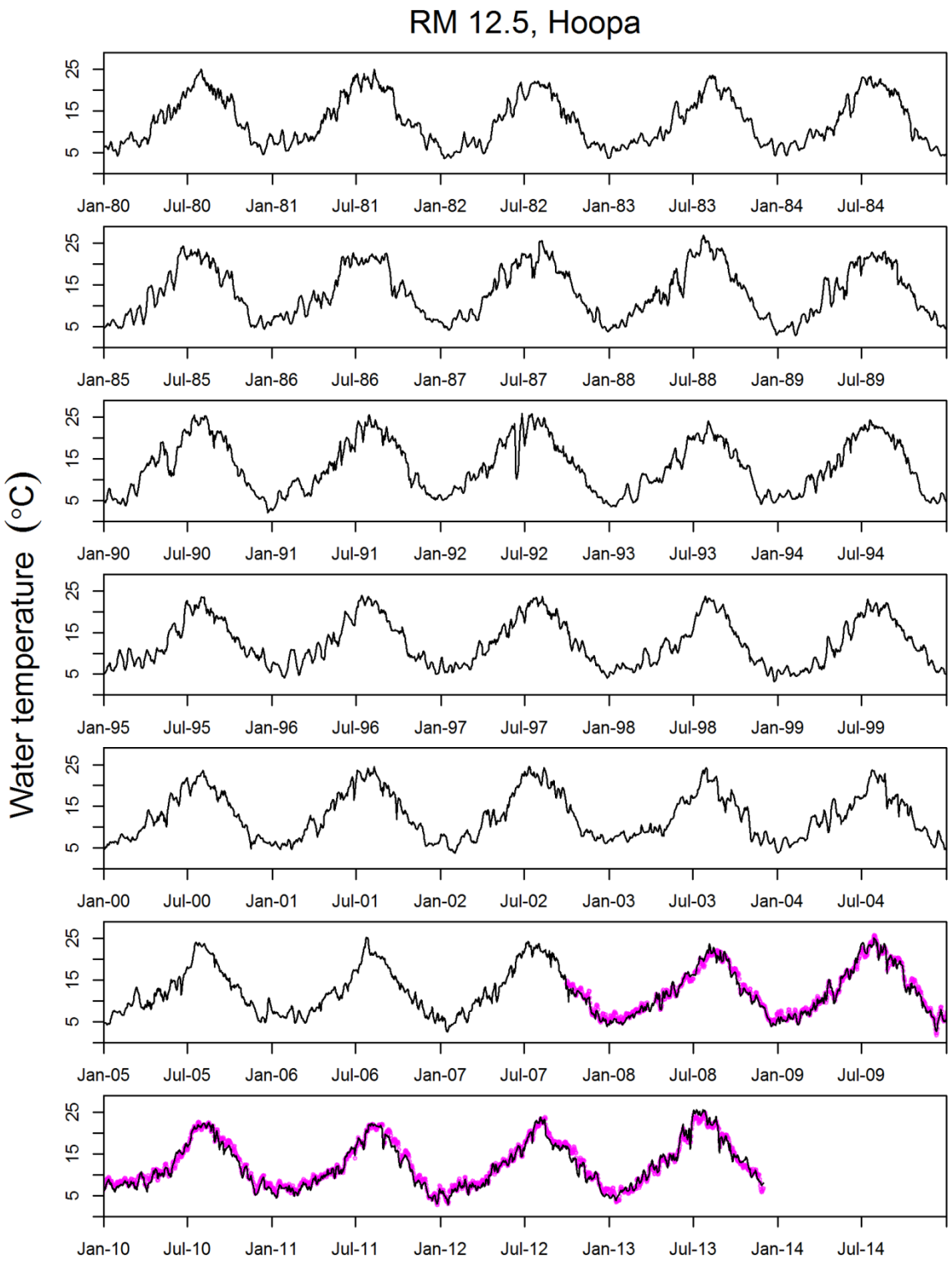

Figure A7. Time series of simulated (solid line) and observed water temperature (o) of the Trinity River at river mile 12.5 at Hoopa.

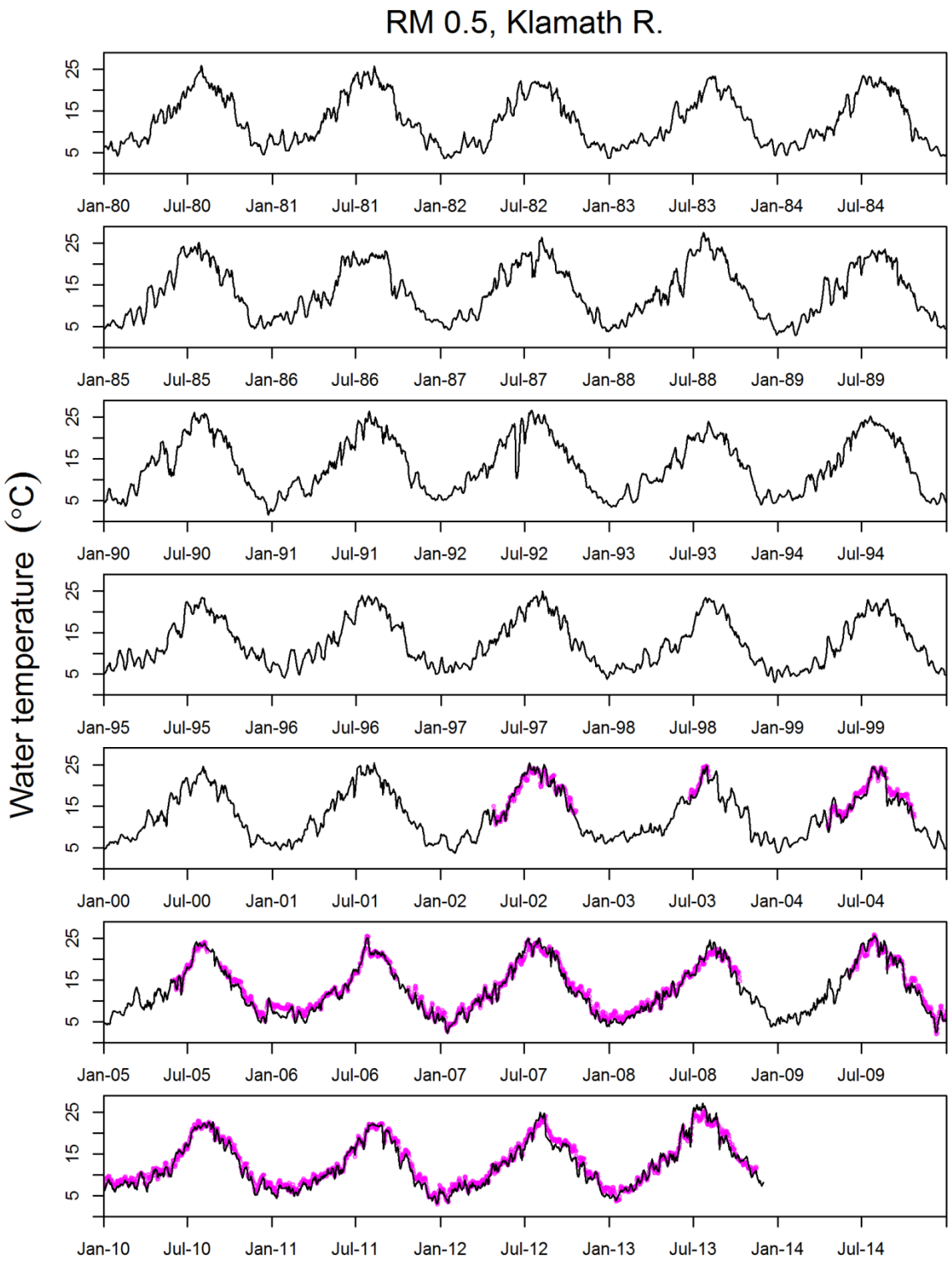

Figure A8. Time series of simulated (solid line) and observed water temperature (o) of the Trinity River at river mile 0.5 near the Klamath River confluence.

Table A3. Year-specific prediction error from the *k*-fold cross-validation.

[Prediction error is estimated by calibrating to observed data without year *k* and then simulating water temperature in year *k*. Statistics are defined as follows: n, number of days with observed water-temperature data, SS, sum of squares; NSS, Nash-Sutcliffe statistic; RMSE, root mean square error; ME, mean error; MAE, mean absolute error]

Reach (r)	Year (*k*)	n	SS	NSS	RMSE	ME	MAE
1	2002	240	13.95	0.966	0.241	-0.052	0.176
	2003	281	11.18	0.977	0.199	-0.089	0.155
	2005	256	14.28	0.974	0.236	0.069	0.169
	2006	365	14.45	0.975	0.199	0.051	0.153
	2007	276	16.30	0.982	0.243	-0.095	0.202
	2008	289	10.10	0.974	0.187	0.017	0.138
	2009	365	13.91	0.988	0.195	-0.002	0.130
	2010	365	11.12	0.987	0.175	-0.054	0.140
	2011	365	29.17	0.964	0.283	-0.093	0.188
	2012	366	52.11	0.939	0.377	0.076	0.260
	2013	296	29.74	0.961	0.317	0.017	0.252
2	2001	16	10.35	0.212	0.804	-0.401	0.713
	2002	183	45.48	0.962	0.499	-0.032	0.405
	2003	99	55.35	0.884	0.748	-0.174	0.562
	2004	139	27.52	0.964	0.445	-0.055	0.337
	2005	177	58.93	0.952	0.577	-0.150	0.460
	2006	269	108.59	0.964	0.635	-0.239	0.493
	2007	276	211.73	0.959	0.876	-0.394	0.719
	2008	289	148.95	0.939	0.718	0.094	0.566
	2009	365	191.85	0.970	0.725	-0.078	0.588
	2010	365	241.95	0.939	0.814	-0.425	0.653
	2011	365	223.85	0.951	0.783	-0.374	0.593
	2012	366	138.81	0.967	0.616	-0.184	0.482
	2013	296	126.39	0.972	0.653	0.151	0.516
3	2001	16	28.84	-0.486	1.343	-0.408	0.841
	2002	239	179.30	0.965	0.866	0.000	0.680
	2003	281	227.39	0.953	0.900	-0.372	0.703
	2004	170	95.44	0.937	0.749	-0.339	0.534
	2005	177	65.18	0.970	0.607	-0.162	0.449
	2006	269	103.52	0.980	0.620	-0.148	0.474
	2007	276	192.18	0.978	0.834	-0.279	0.633
	2008	85	44.74	0.927	0.725	0.077	0.637
	2009	365	250.35	0.976	0.828	0.072	0.666
	2010	365	177.37	0.972	0.697	-0.342	0.553
	2011	365	228.15	0.968	0.791	-0.302	0.600
	2012	366	194.42	0.972	0.729	-0.247	0.573
	2013	296	255.63	0.967	0.929	0.285	0.725

Reach (r)	Year (*k*)	n	SS	NSS	RMSE	ME	MAE
4	2001	13	26.86	-0.543	1.437	-0.604	1.002
	2002	183	123.15	0.953	0.820	0.207	0.673
	2003	99	138.78	0.820	1.184	-0.494	0.877
	2004	170	152.90	0.914	0.948	-0.525	0.719
	2005	256	245.03	0.955	0.978	-0.521	0.779
	2006	365	292.19	0.960	0.895	-0.520	0.692
	2007	276	311.84	0.968	1.063	-0.481	0.839
	2008	289	281.47	0.947	0.987	0.053	0.759
	2009	296	251.94	0.973	0.923	0.053	0.759
	2010	365	279.06	0.961	0.874	-0.550	0.702
	2011	365	322.24	0.960	0.940	-0.457	0.736
	2012	332	283.29	0.956	0.924	-0.210	0.717
	2013	267	253.13	0.970	0.974	0.082	0.736
5	2001	13	24.70	-1.199	1.378	-0.523	0.925
	2002	215	273.71	0.958	1.128	-0.265	0.879
	2003	281	459.58	0.929	1.279	-0.833	1.024
	2005	178	106.09	0.960	0.772	-0.379	0.601
	2006	190	176.25	0.931	0.963	-0.640	0.746
	2007	266	281.13	0.974	1.028	-0.412	0.814
	2008	279	372.37	0.939	1.155	-0.166	0.896
	2009	299	357.23	0.944	1.093	-0.535	0.850
	2010	365	483.35	0.940	1.151	-0.856	0.954
	2011	365	540.05	0.942	1.216	-0.767	0.965
	2012	350	453.59	0.948	1.138	-0.704	0.948
	2013	235	276.23	0.968	1.084	0.390	0.866
6	1999	140	274.70	0.908	1.401	0.360	1.052
	2001	213	213.69	0.934	1.002	-0.302	0.759
	2002	41	23.25	0.437	0.753	-0.557	0.667
	2003	323	364.88	0.953	1.063	-0.517	0.811
	2005	229	266.96	0.957	1.080	-0.569	0.849
	2007	160	75.61	0.981	0.687	-0.042	0.468
	2008	173	143.96	0.958	0.912	0.390	0.689
	2009	141	97.54	0.963	0.832	0.205	0.607
	2010	151	118.47	0.971	0.886	0.063	0.668
	2011	196	100.80	0.979	0.717	-0.170	0.492
	2012	110	29.70	0.969	0.520	-0.286	0.418
7	2007	91	100.71	0.889	1.052	-0.804	0.842
	2008	344	286.34	0.970	0.912	-0.236	0.755
	2009	365	248.01	0.982	0.824	-0.256	0.663
	2010	365	278.45	0.969	0.873	-0.466	0.707
	2011	360	293.43	0.972	0.903	-0.502	0.696
	2012	366	299.84	0.970	0.905	-0.530	0.702
	2013	334	353.20	0.970	1.028	0.307	0.830

Reach (r)	Year (*k*)	n	SS	NSS	RMSE	ME	MAE
8	2002	178	155.80	0.941	0.936	0.077	0.762
	2003	43	48.35	0.832	1.060	-0.906	0.911
	2004	189	347.25	0.861	1.355	-0.780	1.049
	2005	186	177.62	0.964	0.977	-0.599	0.786
	2006	341	322.12	0.966	0.972	-0.560	0.748
	2007	365	312.13	0.977	0.925	-0.321	0.744
	2008	284	288.88	0.966	1.009	-0.268	0.791
	2009	211	227.48	0.972	1.038	-0.204	0.881
	2010	365	312.01	0.966	0.925	-0.614	0.790
	2011	365	298.53	0.972	0.904	-0.610	0.725
	2012	366	488.51	0.952	1.155	-0.749	0.943
	2013	319	396.80	0.965	1.115	0.088	0.887

This page left intentionally blank

Publishing support provided by the U.S. Geological Survey
Science Publishing Network, Tacoma Publishing Service Center

For more information concerning the research in this report, contact the
Director, Western Fisheries Research Center
U.S. Geological Survey
6505 NE 65th Street
Seattle, Washington 98115
http://wfrc.usgs.gov/

ISSN 2331-1258 (online)
http://dx.doi.org/10.3133/ofr20161056